Developmental functions of *rapgef1b* in neural crest specification and presomitic mesoderm patterning

Tuhina Prasad[1,2], Sharada Iyer[1,2], Sian D'silva[1], Reuben J. Mathew[1], Divya Tej Sowpati[1,2], Vegesna Radha[1*], Megha Kumar[1,2, *, #]

[1]CSIR-Centre for Cellular and Molecular Biology (CSIR-CCMB), Habsiguda, Uppal road, Hyderabad-50007, India

[2]Academy of Scientific and Innovative Research (AcSIR), Ghaziabad -201002, India

[*]Correspondence:

vradha@ccmb.res.in, meghakumar@ccmb.res.in

lead corresponding author

meghakumar@ccmb.res.in

Classification: Developmental biology

Keywords: neurodevelopment, zebrafish, *rapgef1*, isoform expression, neural crest, centrosome, presomitic mesoderm, Wnt signaling

Abstract:

Rapgef1, a cell fate determinant and effector of multiple signaling events is essential for mammalian embryonic development. Here, we investigated the developmental role of *rapgef1* using zebrafish as a model. We show that *rapgef1* is maternally expressed and alternately spliced isoforms of its two paralogs, *rapgef1a* and *rapgef1b* show development and tissue-specific expression. CRISPR-Cas9 and morpholino-based targeting of *rapgef1b* resulted in developmental defects in the embryonic brain and somites. The *rapgef1b* morphants showed altered expression of lineage determinants of the cranial neural crest. Comparative transcriptome and altered expression analysis of morphants revealed fresh insights into the developmental functions of *rapgef1b* in presomitic mesoderm, and somitogenesis. During early embryonic mitoses, the morphants showed mitotic defects such as diffused spindle poles and chromosome mis-congression. Our results demonstrate that *rapgef1b* is required for normal embryonic mitoses, cranial neural crest specification, somitogenesis, and myogenesis during embryonic development.

Significance:

RAPGEF1 is an important signaling factor, essential for cytoskeletal remodeling, signaling, and cell adhesion in cultured mammalian cells. The *Rapgef1* knockout mice embryos fail to survive beyond implantation, strongly suggesting its essential role in embryonic development. Further, mutations in *RAPGEF1* are associated with many neurological disorders like schizophrenia and intellectual disability with behavioral defects. However, the role of rapgef1 in regulating embryonic events is poorly understood. This study highlights the developmental functions of *rapgef1* in lineage determination during embryonic development. We show that *rapgef1b* acts as an activator of canonical Wnt signaling and is essential for early neurodevelopment and somite formation. Further, *rapgef1b* is also required to maintain mitotic fidelity, spindle pole integrity, and chromosome congression during embryonic mitoses.

Introduction:

Embryogenesis is a complex, tightly regulated process involving dynamic spatiotemporal gene expression and cytoskeletal remodeling, enabling cell proliferation and differentiation required for organogenesis. As targets of biological signals, Guanine Nucleotide Exchange Factors (GEFs) serve as key signaling centers that activate small GTPases to enable multiple effector functions. RAPGEF1 (C3G), an activator of small GTPases, is predominantly expressed as a 140kD protein, having a catalytic domain at the C-terminus, a central protein interaction domain containing multiple proline-rich stretches (Crk binding region, CBR), and an N-terminal E-cadherin binding domain. Its activity is regulated through intramolecular interactions, phosphorylation, and intermolecular interactions.(Carabias et al. 2020; Radha et al. 2011) RAPGEF1 localizes to the cytoplasm, Golgi, and centrosome, exhibits nucleo-cytoplasmic exchange, and regulates centrosome and cilium dynamics.(Shakyawar et al. 2017; Nayak and Radha 2020; Radha et al. 2004, 2011b; Sriram et al. 2020; Manzano et al. 2021; Shirinian et al. 2010) RAPGEF1 is ubiquitously expressed, interacts with several proteins, and engages in signaling as an enzyme, and as an adaptor.(Shirinian et al. 2010; Dayma et al. 2012; Nayak and Radha 2020; Sriram et al. 2020; Manzano et al. 2021; Radha et al. 2011; Guerrero et al. 1998) Deregulated *RAPGEF1* levels and missense mutations are associated with multiple human disorders.(Hong et al. 2009; Samuelsson et al. 2011; Sequera et al. 2018; Cuesta et al. 2023) More recently *RAPGEF1* has been linked to neurological disorders like schizophrenia and intellectual disability with behavioural defects.(Li et al. 2021; Ryan et al. 2022; Gogos et al. 2021) Some tissue-specific, alternately spliced isoforms of *Rapgef1* have been described, but their functions are yet unknown.(Shivakrupa et al. 1999; Zhai et al. 2001; Voss et al. 2006; Radha et al. 2011; Dayma et al. 2012; Manzano et al. 2021, Verma 2024) A novel brain-specific, longer isoform of *Rapgef1* has recently been reported in adult mouse brains and mature human brain organoids.(Sriram et al. 2020) At the molecular

level, RAPGEF1 interacts with β-catenin in mammalian cells (Voss et al. 2006; Dayma et al. 2012; Sriram et al. 2021) and regulates chromatin dynamics and the expression of cell cycle regulators. *Rapgef1* KO mESCs show enhanced self-renewal and are unable to undergo lineage differentiation.(Voss et al. 2006; Dayma et al. 2012; Shakyawar et al. 2017; Sriram et al. 2021; Vishnu et al. 2015) Studies show that *Rapgef1* knockout mice embryos fail to survive beyond implantation, indicating its essential role in embryonic development. (Ohba 2001; Li et al. 2021) The *Rapgef1* deficient mice with hypomorphic expression of the human allele survive a little longer but show defects in cell adhesion, vasculogenesis, and differentiation.(Voss et al. 2003; Shirinian et al. 2010; Shah et al. 2016; Voss et al. 2008) To summarise, *Rapgef1* is required for cell differentiation events, which form the basis of embryogenesis. In this study, we determine the role of *rapgef1* in early embryonic mitoses and embryonic development. The zebrafish genome contains two *rapgef1* genes, *rapgef1a* and *rapgef1b*. The *rapgef1a* knockdown model in zebrafish showed pan developmental defects, brain, and blood vessel anomalies. The morphants exhibited reduced locomotor capacity, motor neuron defects, and aberrant vasculature. (Li et al. 2021) However, the function of the other homolog, *rapgef1b* has not been elucidated. Here, we delineate the role of *rapgef1b* in regulating tissue specification and patterning during early embryonic development. We demonstrate that *rapgef1a* and *rapgef1b* are expressed in early embryonic stages and show isoform-specific expression during embryogenesis and in the adult zebrafish tissues. Using CRISPR-Cas9 gene knockout and morpholino-based knockdown approach, we show that *rapgef1b* is essential for centrosomal integrity and faithful DNA segregation during early embryonic mitoses. Further, *rapgef1b* plays a key role in cranial neural crest specification, presomitic mesodermal patterning, and somitogenesis.

Results

Rapgef1 is expressed during embryonic development and adult tissues of zebrafish

Zebrafish paralogs, *rapgef1a* and *rapgef1b*, located on chromosomes 8 and 21 respectively, show high homology in the coding regions and encode proteins with similar domain organization (Fig. 1A). Both paralogues contain the highly conserved Crk binding region (CBR) which includes a hotspot for additional exons (orange arrowhead, Fig. 1A). The expression of *rapgef1* during embryonic development and in adult tissues was examined using primers corresponding to the sequence in the 5' end (N-ter), for the amplification of *rapgef1a* and *1b* specific gene products (Fig. 1B, S1A). These primers are common to multiple isoforms that are predicted and amplify products of 130bp and 167bp from *rapgef1a* and *1b* respectively. Semi-quantitative PCR resulted in amplicons of expected sizes from all the developmental stages (32 cell to 2 days post fertilization, dpf). Our results show that transcripts from both paralogs are expressed during early developmental stages such as 32 cell stage, indicating that rapgef1 mRNA is maternally deposited. The *rapgef1* expression continues into the mid-blastula stage (256 cell- 3.3hpf stage) and somitogenesis phase (6 - 21somite stage) until 2dpf (Fig. 1B).

To delineate the spatiotemporal and developmental profile of *rapgef1b*, we used *in situ* hybridization (ISH) with sequence-specific antisense riboprobes, which revealed its ubiquitous expression across developmental stages (red asterisk, Fig 1C), with higher anterior expression at 1dpf (red arrowhead, Fig. 1C). Specificity of the *rapgef1b* expression was confirmed by using sense riboprobes as control (Fig. 1C). Western blotting showed ubiquitous expression of a 150kD polypeptide of Rapgef1, similar to that seen in mammalian cells and tissues, in all the early developmental stages (Fig. 1D). Brain tissue from adult zebrafish prominently expressed a longer polypeptide, compared to the 150kD polypeptide

seen in the heart and liver, indicating tissue-specific expression of alternate isoforms as described earlier using mouse tissues (Fig. S1B) (Sriram et al. 2020)

Differential isoform-specific expression of *rapgef1* in embryonic and adult tissues

A higher molecular weight isoform of RAPGEF1 in the adult zebrafish brain (Fig. S1B) indicates that alternate isoforms including a set of cassette exons may be expressed in zebrafish. Zebrafish *rapgef1* transcripts span 3257bp (*rapgef1a*), 3566bp (*rapgef1b*) and longest variants are composed of 25 (*rapgef1a*) and 28 (*rapgef1b*) exons. Publicly available databases like NCBI suggest the generation of alternately spliced isoforms through the inclusion or exclusion of a pair of exons (10 & 11 in *rapgef1a* and 12 & 13 in *rapgef1b*). Isoform-specific primers for both *rapgef1a* and *1b* which are expected to generate PCR products of different sizes based on the inclusion of one or both exons, were used to study the expression of alternate isoforms (Fig.1E). *Rapgef1a* transcript lacking the additional exons (X4, 405bp product) is expressed throughout embryonic development till early somitogenesis (6 somite stage) (Fig.1F). In contrast, only the smallest isoform lacking exons 12 and 13 (X5, 200bp amplicon) of *rapgef1b* is expressed until 2dpf and its levels decrease as the embryo develops (Fig. 1F). Interestingly, expression of the longer isoforms of *rapgef1a* with 1 or more exons, (X3-498bp, X2-570bp, X1-633bp amplicons) begins with late somitogenesis (18-21 somite stage) (Fig.1F). The longest isoform with exons 10 & 11 is predominantly expressed in the juvenile head and adult brain, with poor expression of other products indicating the isoform-specific function of *rapgef1a* in the adult brain (Fig. S1C). Other adult tissues such as the ovary, heart, liver, and kidney show expression of other isoforms in addition to the embryonic isoform (Fig.1G). Remarkably, there is dynamic isoform switching which results in the expression of the brain-specific, longer isoform of *rapgef1b* containing exons 12 & 13 in the juvenile and adult brain with age (Fig. S1C). Adult tissues such as the

heart, liver, ovary, and kidney predominantly express the isoform lacking cassette exons, with no detectable levels of the longer transcripts of *rapgef1b* (Fig.1G). We also investigated the expression patterns of brain-specific isoforms by ISH with sequence-specific antisense riboprobe (Fig. S1D). *Rapgef1b* (antisense riboprobe to exon 3 and 4) is expressed in the diencephalon (double red asterisk), rods, and cones (red arrow), ganglion cell layer (red arrowhead), gut, and myotomes of 3dpf larvae (red asterisk) (Fig. S1D). In contrast, the brain-specific isoform expression is restricted to the diencephalon, and ganglion cell layer of the eye but is absent in rods and cones and myotome (red arrow, Fig.S1D). Thus, the expression of the brain-specific isoform of *rapgef1b* is restricted to the cranial region and absent from mesodermal-derived tissues like myotome.

Rapgef1b is required for neurodevelopment and anteroposterior axis patterning

To determine the functional role of *rapgef1b* in embryogenesis, we used a knockdown approach using sequence-specific antisense morpholino (ATG/ translational blocker) and a CRISPR-based knockout approach against z*Rapgef1b* (Fig 2A). The *rapgef1b* morpholino morphants showed depletion of Rapgef1 protein and the *rapgef1b* KO fish showed a deletion of 366bp, confirming effective abrogation of function (Fig. 2C, S2A). The morphants were characterized as P0 (normal, similar to WT), P1 (brain and axis defects), and P2 (severe brain and axis deformities) (Fig. 2B, 2D, S2D). *Rapgef1b* depletion by both strategies resulted in defects in the brain, eye, and inner ear at 1dpf (red asterisk, Fig. 2B). The morphants also showed somitic defects (red arrowhead, Fig.2B) and anterior-posterior body axis abnormalities (red arrow, Fig. 2B). The severity of the phenotype and the survival rate were observed in a morpholino concentration-dependent manner with time (Fig. 2B, C). To ascertain that the phenotype was specific to *rapgef1b* knockdown, we performed rescue experiments by introducing human *rapgef1* mRNA, which resulted in partial, but significant

rescue (39%) of the severe phenotype, P2 (Fig. 2D, E). In contrast, human *rapgef1* mRNA of a predicted deleterious mutant Y485C (Mutagenetix & ClinVar), a residue conserved in zRAPGEF1, that shows altered stability and compromised phosphorylation by Abl (unpublished findings from our lab) could not rescue the *rapgef1b*-specific phenotype (Fig. 2D, E*).* These results suggest that *rapgef1b* is essential for early development and morphogenesis of the brain, eye, somites, as well as the elongation of the body axis.

Rapgef1b is required for cranial neural crest specification, formation of neural crest derivatives, and maintenance of head size

As *rapgef1b* is expressed in early development and its depletion resulted in severe defects in the brain and anteroposterior axis, we inferred that *rapgef1b* is required for early neurodevelopment and axis specification. To test this hypothesis, we performed gene expression analysis of key neural crest specification markers and patterning on *rapgef1b* morphants (morpholino injected) and mutants (CRISPR-based knockouts). The morphants/mutants showed a significant reduction in neural crest specifier genes, *twist1a* (red asterisk, Fig. 3A) and *sox2* (red arrowhead, Fig. 3D). *Twist1a* is expressed in the cranial neural crest-derived head mesenchyme, diencephalon and is required for the migration of neural crest cells and their differentiation. (Yeo et al. 2007) *Sox2* is required for otic and epibranchial placode induction, promotes the maintenance of pluripotency, and regulates the development of the sensory epithelium and neural tube. (Gou et al. 2018) (Asad et al. 2016) (Hagey et al. 2018) . The reduced expression of specifier genes *twist1a* and *sox2* strongly indicate that *rapgef1b* plays a key role in the maintenance of progenitor population in the neural crest, sensory placodes and is involved in neural tube patterning. We also observed a reduced expression of *sox10* in the head (red arrow, Fig. 3B). The expression was rescued in the morphants injected with human *Rapgef1* mRNA (red arrowhead, Fig. 3B). *Sox10* marks

the undifferentiated cranial neural crest and regulates the specification, maintenance of the progenitor pool and migration. (Dutton 2001; Drerup et al. 2009; Asad et al. 2016; Nagao et al. 2018) Loss of *sox10* results in cell death and failure to undergo differentiation to form CNS and craniofacial cartilage, bone, etc. (Carney et al. 2006; Delfino-Machín et al. 2017) We also observed increased cell death in the anterior region of the embryo (forebrain, midbrain-hindbrain boundary/ MHB, and midbrain) as shown by acridine orange staining (white asterisk, Fig. S3A). These results suggest that pre-migratory neural crest cells marked by *sox10* expression are lost in the morphants and may be the underlying cause of a poorly developed brain (Fig.2B).

Other key regulators of specification, differentiation, and morphogenesis are the *Pax* family members. *Pax2a* is expressed in the eye, MHB, otic placode, and the pronephros. (Hans et al. 2004; Mackereth et al. 2005; Lusk and Kwan 2022; Tan et al. 2023) *Pax2a* along with *pax8* is required to maintain otic cell fate and high levels of *pax2a* promote otic differentiation. (McCarroll et al. 2012) The *rapgef1b* morphants exhibit an expansion of *pax2a* expression domains in the eye, otic vesicle, and MHB (red asterisk, Fig.3C) Thus, *rapgef1b* is essential to maintain progenitor cell fate, and its depletion results in an increase in differentiation-inducing signals such as *pax2a*. Concomitantly, we also observed an upregulation of *egr2b*, which is rhombomere 3 and 5 specifier in the segmented hindbrain. (Fig. S3B) ((Maves and Kimmel 2005; Oxtoby and Jowett 1993; Seitanidou et al. 1997; Thierion et al. 2017) We also examined if *rapgef1b* is essential for neuronal differentiation. Neuronal nuclei (NeuN) mark the post-mitotic neurons as it is distributed in the nuclei of mature neurons of the CNS. Thus, NeuN marks terminal differentiation and determination of neuronal phenotype. (Duan et al. 2016; Won et al. 2016) The morphants showed a decrease in NeuN-positive cells (red asterisk, Fig.3E), indicating that depletion of *rapgef1b* results in the decrease of post-mitotic

mature neurons and strongly indicates its role in terminal neuronal maturation and differentiation.

At larval stages of development (4-5dpf), the *rapgef1b* morphants exhibited severe craniofacial skeletal anomalies, defects in the Meckel's cartilage, and lack the ceratobranchial skeletal elements (red asterisk, Fig.3F). Craniofacial skeletal elements are derived from the cranial neural crest, and the mesenchyme is derived from sclerotome and lateral plate mesoderm. (Yang et al. 2011) The *rapgef1b* depleted embryos showed a reduction in *sox10* positive neural crest cells, which may be the underlying basis of the observed craniofacial defects. Thus, *rapgef1b* plays a key role in the maintenance of the undifferentiated neural crest population which gives rise to the craniofacial skeletal elements. Further, the morphants showed microcephaly-associated craniofacial features such as reduced overall head area (HA), interpupillary distance (IPD), and iris distance (ID) (Fig. 3G). To determine the cellular basis of the small head phenotype, we examined the role of *rapgef1b* in embryonic mitoses. Previous studies show that RAPGEF1 localizes to the centrosome and regulates centriole duplication during the cell cycle in cultured mammalian cells. (Nayak and Radha 2020) The morphants exhibited severe centriolar and spindle defects, showing that *rapgef1b* is required to maintain spindle pole integrity in early embryonic mitoses (Fig. 3H). The morphants showed severe pericentriolar matrix and centriolar defects as shown by γ tubulin (white asterisk, Fig.3H) and centrin 3 respectively (Fig. S3C). The *rapgef1b* depleted embryos also showed elongated spindle length (red dotted line, Fig. 3H) and chromosome congression anomalies at metaphase (Fig. 3H). These defects are likely to result in impaired mitotic progression and chromosome instability in *rapgef1b* morphants. This is also indicated by an overall decrease in *plk* transcript levels (Fig. S3D), essential for mitotic progression, faithful segregation of chromosomes, and proper spindle assembly. (Jeong et al. 2010).

These results reveal that the centrosomal functions of *rapgef1* are also conserved during embryonic mitoses in zebrafish in a manner akin to the mouse and human cells.(Nayak and Radha 2020)

Rapgef1b **plays an important role in paraxial mesoderm differentiation**

To further explore the developmental functions of *rapgef1b*, we performed transcriptome sequencing analysis to identify novel pathways contributing to the observed phenotypes, differentially expressed genes (DEGs), and enriched processes in the *rapgef1b* morphants. The principal component analysis (PCA) and correlation matrix showed variance and the agreement of the three replicates across conditions (Fig. S4A, B). The volcano map showed the distribution of DEGs, 76 genes were downregulated and 106 genes were upregulated at the transcriptional level with clear patterns of clustering in the *rapgef1b* depleted embryos within the FDR adjusted p-value <= 0.05 (Fig. 4A). The altered DEGs are listed and their P values are shown in (Fig. S4C). We also performed GO pathway analysis to further investigate the functional relationships between the DEGs. Gene ontology analysis showed an enrichment of anterior/posterior pattern specification, somite development, segmentation, and mesodermal morphogenesis genes indicating that *rapgef1b* plays a key role in paraxial mesoderm specification, patterning and differentiation (Fig. 4B). The heat map shows the selected up-regulated and down-regulated genes in these mentioned processes (Fig. 4C). To validate the transcriptome analysis, we assayed transcript levels of some of the up and down-regulated genes in control and *rapgef1b* morphants (Fig. 4D-J). The *rapgef1b* morphants showed increased transcript levels of the up-regulated group of genes –*msgn1*, *tbx16*, and *bbc3*. *Mesogenin 1* (*msgn1*) and *tbx16* (*spadetail*) induce the differentiation program in the PSM cells by reducing the expression of progenitor maintenance markers such as *fgf8* and *ntl* and induces the expression of *tbx6*. Hence, *msgn1* is essential to regulate progenitor pool

population until somitogenesis is complete.(Fior et al. 2012; Chalamalasetty et al. 2014) The upregulation of *msgn1* and *tbx16* in *rapgef1b* morphants by transcriptomic analysis strongly suggests that progenitor fate is suppressed and an untimely differentiation program is initiated upon *rapgef1b* depletion (Fig. 4D). We also observed up regulation of intrinsic apoptotic genes such as *bbc3* (*puma*) in our transcriptome analysis and qPCR validation (Fig. 4E).(Wang et al. 2021; Jin et al. 2011) Hence, pro-apoptotic mRNAs are upregulated in the *rapgef1b* morphants which result in increased apoptotic cells marked by acridine orange in the cranial region of *rapgef1b* morphants (Fig. S3A). In contrast, *rapgef1b* morphants showed reduced transcript levels of skeletal muscle genes such as *myhc4*, *myoz1b*, and *pvalb3* (Fig. 4F). (Bryson-Richardson et al. 2005; Liu et al. 2022; Housley et al. 2014) Further, *her13* which is required for the formation of all somitic borders was also downregulated in *rapgef1b* morphant transcriptome (Fig. 4G), forming the underlying basis of disrupted somite architecture (red arrow, Fig. 2B).(Sieger et al. 2006) Hence, transcriptome analysis reveals that *rapgef1b* plays a crucial role in the development of paraxial (somitic) mesoderm and its derivatives.

Rapgef1b **is required for presomitic mesoderm patterning, somitogenesis and myogenesis**

Transcriptome analysis revealed that *rapgef1b* plays an important role in somitogenesis and mesoderm development. Hence, we examined somite development and the myogenic program in *rapgef1b* morphants. The phalloidin 568 staining showed disruption of the F-actin fibres in the muscle of the *rapgef1b* morphants (Fig. 5A) (Goody 2013). To ascertain the role of *rapgef1b* in myogenesis and somite patterning, we examined the morphants for *myoD1* expression. *MyoD1* is expressed in the somites and is required for the establishment and maintenance of somite-derived muscle progenitor lineages. (Pownall et al. 2002; Weinberg et

al. 1996) *Rapgef1b* morphants showed defects in the somite organization and architecture. The somites appeared enlarged and irregular with imperfect boundaries (red arrowhead, Fig.5B) as compared to the periodic and sharp somite boundaries in control (red dotted line, Fig. 5B). These somitic defects were rescued in the morphants injected with h*Rapgef1* mRNA (Fig. 5B). We also examined patterning of the somitic mesoderm. *Tbxta* is expressed in the mesoderm during early development and neuromesodermal progenitors that give rise to the spinal cord and paraxial mesoderm of the trunk and tail. At later stages, *tbxta* expression is restricted to the notochord and tailbud. (Hug et al. 1997; Griffin et al. 1998; Shimizu et al. 2005; Gladysheva et al. 2021; Kinney et al. 2020) The 1dpf morphants showed notochordal defects and expanded expression of *tbxta* in the tailbud (red arrowhead, Fig. 5C). The diffused and disrupted somitic boundaries were also observed at the early somitogenic phase (red arrowhead, Fig. 5D) coupled with and loss of segmental *myoD1* expression (red asterisk, Fig. 5E). We also observed reduced expression of *myoD1* in the PSM at the bud stage, indicating that *rapgef1b* depletion resulted in impaired presomitic mesoderm (PSM) patterning (red arrow, Fig. 5E). Further, we observed expanded *tbxta* expression at the bud and 6 somite stage as well (red arrow, Fig.5F) which suggests that neuromesodermal progenitor pool is maintained in the morphants and *rapgef1b* is required to induce mesodermal differentiation.

Somites are derived from the segmentation of the PSM under the regulation of the oscillatory gene network which involves *her* genes, Wnt, notch, and FGF signaling.(Sieger et al. 2006; Trofka et al. 2012) *Her1* and *her7* are expressed as two stripes in the PSM, tailbud, and are essential for somite formation. (Holley et al. 2000) *Her* deficient embryos show enlarged somites with weak boundaries. Both these genes have partial functional redundancy, yet *her1* is important for the formation of anterior somites and *her7* for posterior somites.(Henry et al.

1063; Choorapoikayil et al. 2012; Schröter et al. 2012) The *rapgef1b* morphants show a lack of *her1* expression in the anterior somites in a two-stripe manner as compared to control (red asterisk, Fig.5G). At later stages, the embryos also showed reduced expression in the tail region (red arrow, Fig. 5G). We also observed reduced expression of *her7* in the anterior somites and PSM (red arrow, Fig. 5H). Thus the loss of segmental stripes of *her1* and *her7* suggests that the segmentation clock is disrupted in the PSM of *rapgef1b* morphants. *Papc* (paraxial protocadherin), expressed in dorsal mesodermal cells during gastrulation contributes to the convergence movements and PSM.(Kim et al.; Amacher 2002; Harrington et al. 2007; Weiser et al. 2009) The anterior somites (red asterisk, red arrowhead, Fig. 5I) and PSM expression of *papc* is absent in the morphants (red arrow, Fig. 5I). Further, *papc* positive cells in the paraxial mesoderm are not detected in the tailbud of morphants at somite stage (red arrowhead, Fig. 5I). This downregulation of *papc* in *rapgef1b* depleted embryos suggests impaired convergence movements in the mesoderm, ultimately resulting in somitic defects. Another PSM marker, *fgf8* plays a key role in PSM maturation and somite formation.(Carraco et al. 2022) *Rapgef1b* morphants show an expansion of *fgf8* expression in the midbrain-hindbrain boundary at the bud stage (red asterisk, Fig.5J). At later stages, posterior somites appear enlarged with imperfect somitic boundaries (red arrowhead) and expanded expression in the head (double red asterisk) and tailbud (red arrow, Fig. 5J).

***Rapgef1b* regulates mesoderm specification by modulating canonical Wnt signaling**

Early mesodermal cell fate is regulated by the *cdx* family and it also plays key roles in axial elongation, anteroposterior patterning, and the development of the trunk and tail.(Foley et al. 2019) Differentiation of paraxial mesoderm and somitogenesis also requires other *tbx* family members along with Wnt and FGF signaling (Henry et al. 1063; Hofmann et al. 2004; Kinney et al. 2020) (Szeto and Kimelman 2004; Lou et al. 2006) *Cdx4* is also an early trunk neural

crest specifier, expressed in the trunk neural crest cell progenitors and the developing tailbud.(Shimizu et al. 2005; Rocha et al. 2021) Interestingly, *rapgef1b* depleted embryos show an upregulation of *cdx4* transcript levels by qPCR and *in situ* hybridization (red asterisk, Fig. 6A), suggesting that trunk neural crest cells are maintained in the progenitor fate in the morphants. So, *rapgef1b* is essential to initiate differentiation fate in the trunk neural crest population. Our results show that *rapgef1b* is essential to maintain progenitor cell fate of the cranial neural crest population in the anterior embryo (Fig.3). However, it is required for the initiation of the differentiation fate in the mesodermal lineage in the posterior embryo (Fig.6A). We also observed an overall increase in *tbx6* transcripts in the morphants, particularly in the tailbud region (red arrowhead, Fig. 6A). *Tbx6* plays important role in the specification of paraxial mesoderm, somite patterning, and myogenesis. (Chapman et al. 1998; Hofmann et al. 2004; Wittler et al. 2007) Studies show that ectopic *tbx6* expression promotes less mesodermal fate. (Kinney et al. 2020) This increase in *tbx6* expression levels results in reduced mesodermal fate and may be the underlying cause of the failure of somite segmentation in the tailbud mesoderm.

To investigate the underlying cause of *tbx6* upregulation, we examined the Wnt signaling pathway in the *rapgef1b* morphants. Wnt signals are required for mesoderm induction, somite formation, and patterning through the β-catenin-Lef1/TCF pathway.(Henry et al. 1063; Hofmann et al. 2004; Kinney et al. 2020) The abrogation of canonical Wnt signaling impairs somitogenesis and presomitic segmentation.(Hofmann et al. 2004; Wittler et al. 2007) Indeed, during early embryonic stages, we observed a decrease in the Wnt signaling effector β-catenin in the nucleus and cortex in interphase and mitotic phase (white asterisk, Fig. 6B). Western blotting showed a reduction in phospho GSK-3β levels (ser9) and total β-catenin levels in *rapgef1b* morphants (Fig.6C). The phospho β-catenin levels (ser33/37) was

increased in the morphants (Fig. 6C), indicating proteosomal degradation of β-catenin and downregulation of Wnt signaling. The *rapgef1b* depleted embryos also showed decreased transcript levels of Wnt effectors *axin2*, *lef1*, and *cyclin D1*, suggesting the downregulation of canonical Wnt responses in morphants (Fig.6D). To probe the *rapgef1b* mediated Wnt signaling, we exposed morpholino injected embryos with Wnt activator CHIR99021 or Wnt inhibitor XAV939 (Fig. 6E). Exposure to Wnt inhibitor resulted in increased number of *rapgef1b* P1 and P2 phenotypes (red arrow, Fig. 6E) and rescued by administration of h*rapgef1* mRNA. In contrast, morphants when exposed to the Wnt activator exhibited normal morphology, classified as P0 (blue arrow, Fig. 6E). Further, inhibition of Wnt signaling also results in reduced axis elongation(Bajard et al. 2014), which is consistent with the reduced Wnt signaling in *rapgef1b* morphants resulting in shortened body axis. To summarise, the *rapgef1b* depletion reduces canonical Wnt signaling, which is the underlying basis for the impaired mesodermal patterning and somitic defects.

Discussion and future perspectives:

Embryogenesis involves cell fate specification from progenitors and subsequently differentiation. As *rapgef1* plays crucial roles in cell adhesion, cytoskeletal organization, and cell proliferation, it is poised to play key roles in embryonic development. Despite the plethora of literature on *rapgef1* functions, its role in embryogenesis is poorly understood as murine embryos lacking *rapgef1* fail to survive beyond implantation. Hence, we chose to explore the developmental functions of *rapgef1* in zebrafish embryos, which have two paralogs *rapgef1a* and *rapgef1b*. A recent study highlighted the role of *rapgef1a* in vasculogenesis and CNS development of larval zebrafish. (Li et al. 2021) However, the role of *rapgef1b* remains unknown. In this study, we elucidate the developmental functions of *rapgef1b* in early embryonic events of the lineage specification in the neural crest and

paraxial mesoderm (Fig.7). Our results provide the first evidence for temporal and tissue-specific expression of multiple alternately spliced isoforms from the duplicated zebrafish *rapgef1* genes. We observed an isoform-switching event of *rapgef1a* and *rapgef1b* from embryonic stages and the expression of a longer brain-specific isoform in larval and juvenile stages. The difference in gene expression of the two paralogues of *rapgef1* suggests functional distinction of their products during development and in various adult tissues. Tissue-specific alternate splicing occurs at a hot spot which is conserved across vertebrate species, and results in the inclusion of one or more exons. Switching of *rapgef1* isoform expression during the differentiation of tissues is likely a mechanism to fine-tune GTPase activity and signaling mediated by intermolecular interactions during developmental stages. The shorter isoform of *rapgef1b* is predominantly expressed at stages of brain development when neural progenitor cells are proliferating, and the longer isoform containing cassette exons is predominant in the adult brain where the majority of cells have differentiated. To summarise, variation in tissue-specific and temporal expression of alternately spliced products with differing properties enables regulation of lineage-specific differentiation in the embryo. Future studies to delineate the isoform-specific roles of the *rapgef1* transcripts during embryogenesis will help us understand the transcriptional regulation of *rapgef1* and the isoform-specific functions on neural tissue specification and patterning.

Further, we elucidated the functions of *rapgef1b* in early embryonic mitoses and lineage specification in the cranial neural crest. The morphants showed smaller head size and a decrease in the expression of neural crest specifier genes, suggesting that *rapgef1b* is required to maintain the progenitor fate in the cranial neural crest. As mammalian *RAPGEF1* is a known regulator of centrosomal and cytoskeletal dynamics, optimal Rapgef1b levels may be necessary to maintain early embryonic cell divisions. To potentiate this hypothesis, we show

that *rapgef1b* is required for the maintenance of spindle pole integrity during early embryonic mitoses. Further, the enhanced apoptosis seen in morphants may be a consequence of impaired mitosis. The reduced head size, shortened interpupillary distance, and mitotic aberrations coupled with increased apoptosis allude to a microcephaly-like phenotype in *rapgef1b* morphants. Hence, it is imperative to delineate the mitotic regulation by *rapgef1b* in the embryonic brain to gain mechanistic insights into its neurodevelopmental functions.

In addition to brain development, RNAseq and detailed gene expression analysis revealed that *rapgef1b* is also required for paraxial mesoderm patterning, somitogenesis, and the establishment of the body axis. *Drosophila rapgef1* is expressed in the somatic and visceral muscles and plays a key role in muscle development. It is required to form the muscle architecture and maintain somatic muscle integrity in the larval stage.(Marada et al. 2016; Shirinian et al. 2010) Intriguingly, zebrafish *rapgef1b* mutants also showed notochordal and somitic defects. The *rapgef1b* depleted embryos also showed reduced expression of PSM genes indicating that PSM segmentation is disrupted. The expression of these genes is also reduced or virtually absent in the anterior somites. The PSM is derived from the trunk mesodermal progenitors and these progenitor cells are maintained in an undifferentiated state by activation of Wnt signaling and *tbxta* expression.(Szeto and Kimelman 2006; Yabe and Takada 2012) Thus, canonical Wnt signals are key regulators of PSM maturation and somite formation by regulating the expression of lineage determinants.(Carraco et al. 2022) Our results using pharmacological inhibitors and activators of Wnt, is suggestive of *rapgef1b* products acting through modulation of GSK3β and βcatenin signaling. The *rapgef1b* depletion results in the down-regulation of Wnt signals, disrupting the balance between proliferation and differentiation, inducing premature pro-differentiation signals in the mesodermal progenitor cells. Hence, *rapgef1b* morphants show disrupted PSM specification

and defects in somite organization and architecture. Further, *rapgef1b* morphants also show increased apoptosis in the embryonic CNS. Reports show that lack of Wnt signals results in extensive apoptosis in the midbrain and cerebellum during the somitogenesis phase.(Buckles et al. 2004; Diez del Corral and Morales 2017; Kinney et al. 2020) In summary, we establish that *rapgef1b* plays an essential role in the lineage specification of cranial neural crest and presomitic mesoderm by modulating Wnt signaling. Also, the nature of the interaction between *rapgef1b* and developmental signaling pathways will provide valuable insights into the molecular functions of *rapgef1b*. Further, as lineage specification is also regulated by chromatin remodeling, it will be interesting to determine if and how *rapgef1b* regulates chromatin modifications to alter the expression of lineage determinants.

Materials and Methods:

Zebrafish lines, MO injection, and characterization of phenotypes

Tubingen strain (TU-AB) zebrafish were raised according to standard protocols as described earlier. All experiments were performed according to protocols approved by the Institutional Animal Ethics Committee of the Council of Scientific and Industrial Research, Centre for Cellular and Molecular Biology, India. Embryos were obtained from the natural spawning of adult fish, kept at 28.5°C, and staged according to hours after fertilization. (Kimmel et al. 1995) (The endogenous *rapgef1* levels were depleted by using MO (*rapgef1b* translation blocker, 5'-CTTGCTTTCTATTTTCCCCGACATG-3′ (Gene Tools)**,** 0.25mM, 0.5mM and 1mM in each embryo and standard control MO, 5′-CCTCTTACCTCAGTTACAATTTATA-3′ (Gene Tools), 0.25mM, 0.5mM and 1mM was used as negative controls. For rescue experiments, 50pg of human RAPGEF1 mRNA was co-injected along with *rapgef1b* MO in each embryo at the one-cell stage. The embryos were then analyzed for gross morphological defects, and survival at later stages of development (1dpf).

Generation of the r*apgef1b* knockout line

Single guide RNAs (sgRNAs) targeting *rapgef1b* (Ensembl ID: ENSDART00000123759.3) for CRISPR/Cas9-mediated knock-out were designed using CRISPOR online tool (www. https://crispor.tefor.net/). Two sgRNAs targeting the exons 3 and 4 of the *rapgef1b* gene were used with the following target sequences: 5′-GAGATACTTTAAGACGATTG -3′ and 5′-GCTTGGCGACTCTGATTCGC-3′. Gene-specific oligos were annealed in a PCR machine, ramping temperature down from 95°C to 4°C in a stepwise manner and run on agarose gel electrophoresis to ensure correct annealing. Both the sgRNAs were cloned into pDR274 plasmid (Addgene #42250). RNAs from both clones were *in vitro* transcribed using the Maxiscript SP6/T7 kit (AM1322) according to the manufacturer's instructions. One-cell stage

zebrafish embryos were injected with 3nl of a solution containing 600pg of Cas9 protein (TrueCut™ Cas9 Protein v2 #A36498) and 150pg of each sgRNA. The CRISPR/Cas9 approach generated a deletion of 366 bp, resulting in a premature STOP codon in exon 4. For genotyping, genomic DNA was obtained by incubating the samples (whole embryos or adult caudal fin fragments) in TE buffer supplemented with 1mM EDTA and 10 µg/ml Proteinase K (Cat no. 193981) for 1 h (embryos) or 4 h (fins) at 55 °C and 10 min at 95 °C, and then stored at 4 °C. Primers sequences used for genotyping can be found as Table S1. (Franke et al. 2021)

RNA isolation, Semi-quantitative RT-PCR, and sequencing

Total RNA was isolated from 100 embryos for each group using the RNA isolation kit (MN; 740955.50) as per the manufacturer's protocol. Total RNA from various zebrafish adult tissues was prepared using RNAiso Plus (TaKaRa, cat. no. 9109) according to the manufacturer's protocol. cDNA was synthesized from total RNA using PrimeScript 1st strand cDNA synthesis kit (TaKaRa, cat. no 6110A). PCR was carried out using the prepared cDNA for amplification of zebrafish *rapgef1* isoforms and *rpl7* (internal control). Zebrafish isoform-specific primers for *rapgef1a* and *rapgef1b* were used to identify splice variants of these isoforms present in embryonic and adult zebrafish tissues. All primers used in this study are listed in Fig. S2. PCR was performed in BioRad C1000 Touch thermal cycler with, Taq DNA Polymerase (TaKaRa, cat. no. R500A). The following PCR conditions were used for amplification of *rapgef1*: initial denaturation was at 94 °C for 5 min, followed by 30 cycles of denaturation at 94 °C for 30 secs, annealing at 60°C for 30 secs, and extension at 72 °C for 30 sec. The final extension was for 10 min at 72 °C. Amplified PCR products were examined and pictures were captured using the Vilber-Lourmat Gel Documentation system (Germany). The PCR fragments were eluted using Macherey-Nagel NucleoSpin Gel and PCR clean-up

kit (MN; 740609.50) as per the manufacturer's protocol and sequenced to confirm that the amplicons are generated from alternate splice variants.

Antisense riboprobe preparation

For cloning sequence-specific exonic fragments to synthesize riboprobes, total RNA was isolated from 1dpf embryos of the TU-AB strain using an RNA isolation kit (MN; 740955.50). The total RNA was used to prepare cDNA using the PrimeScript 1st strand cDNA synthesis kit (TaKaRa, Cat. # 6110A). Sequence-specific primers were used to amplify the specific gene fragment and cloned into the pGEMT easy vector and the sequence was verified. The sequence-verified plasmid was linearised using Nco1 and antisense digoxigenin (DIG)-labeled riboprobes were synthesized using the DIG RNA labeling kit (Roche #11175025910). (Iyer et al. 2023)

Whole Mount RNA in Situ Hybridization

Embryos of various stages were fixed in 4% paraformaldehyde overnight followed by methanol fixation. Methanol-fixed embryos were rehydrated with 50% MeOH/PBT (1× PBS and 0.1% Tween 20). Embryos were rinsed with PBT, a 1:1 PBT/hybridization wash, and then a hybridization wash (50% formamide, 1.3 × SSC, 5 mM EDTA, 0.2%, Tween-20, H2O). Embryos were incubated with a hybridization mix (50% formamide, 1.3 × SSC, 5 mM EDTA, 0.2%, Tween-20, 50 µg/mL yeast t RNA, 100 µg/mL heparin, H2O) for 1 h at 55 °C. The riboprobes prepared in the hybridization mix were added and incubated for 16 h at 55 °C. Then, embryos were rinsed with prewarmed hybridization wash for 30 min (2 times) at 55 °C and followed by 1 × TBST wash (5 M NaCl, 1 M KCl, 1 M Tris, pH 7.5, and 10% Tween 20) at room temperature. Then, blocking was done with 10% FBS heat-inactivated fetal bovine serum (Gibco; 16210-064) for 1 h at room temperature. The embryos were then incubated

with an Anti-DIG-AP antibody (Roche 11093274910) with a dilution of 1:5000 overnight at 4°C. The next day, embryos were transferred into a 6-well plate and washed twice with 1X NTMT (0.1M NaCl, 0.1 M Tris-Cl at pH 9.5, 0.05M MgCl2, 1% Tween-20 and H2O) for 10 min; then, incubated with 1:1 NBT-BCIP solution (Cat no. PI34042) NTMT solution for the color development. The embryos were monitored during this color reaction and stopped with 1× PBT as a stop solution. Images of embryos were captured using a Zeiss Stemi 2000CVR bright-field microscope at 5× magnification (with AxiocamICc1)(Schulte-Merker et al. 1992) The embryos after *in situ* hybridization at 3dpf were cryoprotected with 30% sucrose in PBS, embedded in Tissue freezing medium (Leica) and cryosectioned at 15 µm thickness.

Western Blot analysis

Whole zebrafish embryos (n=100) and adult tissues were homogenized using RIPA buffer (20mM Tris–HCl, pH 7.4; 150mM NaCl; 5mM EDTA; 1% NP-40; 0.4% sodium deoxycholate, 0.1% SDS and 1× Protease inhibitor cocktail) and kept on ice for 15min with vortexing 3 times. The homogenized lysates were centrifuged (12000 rpm for 20 min at 4°C), and supernatant were taken for the analysis. Subsequently, samples were boiled in 1× Laemmli buffer and subjected to SDS-PAGE. 20 µg of total protein was loaded in each lane on 8% SDS-PAGE gel for detection of endogenous proteins. Proteins were transferred to PVDF membranes (Merck Milipore, ISEQ00010) by electro-blotting. Membranes were blocked for 2 h at room temperature in TBST (20 mM Tris HCl, pH 7.5, 150 mM NaCl, 0.1% TWEEN 20) containing 3% BSA and probed overnight with primary antibodies (Fig. S3, Table S2). After three washes with TBST, the blots were incubated with HRP-conjugated secondary antibody for 1 hr, and then washed in TBST. The blot was developed for chemiluminescence signal using the chemiluminescence (Bio-Rad) and captured in the Vilber-Lourmat Chemiluminescence System (Germany). Densitometry analysis was done

using Image-J. β-Tubulin was used as a control for the normalization of protein in all the samples. The data were plotted as mean normalized protein level relative to WT± SD was plotted as error bar. Data from at least three independent experiments were plotted and significance was calculated with unpaired t-test using Prism 8.0.

Real-time PCR

For quantitative real-time PCR (RT-PCR), we performed PCR using Power SYBR Green PCR Master Mix (Applied Biosystems) with ViiA 7 Real-Time PCR System (Applied Biosystems) according to the manufacturer's instructions. Quantification data are represented as means ± SEM of three independent experiments. Analyses on normalized data were performed using the 2−ΔΔCT algorithm (the delta−delta-Ct or ddCt algorithm). All genes were normalized against z*rpl7* unless mentioned otherwise. The GraphPad Prism software was used for the analysis. For the statistical significance of the data, p-values were calculated by performing an unpaired Student t-test. All primers used in this study are listed in Table S1.

Immunohistochemistry of zebrafish embryos

Embryos of various stages were fixed in 4% paraformaldehyde overnight followed by methanol fixation. Methanol fixed embryos were rehydrated with 50% MeOH/PBST (1X PBS and 0.1% Triton X-100) followed by incubation in blocking solution 1% BSA/PBST for 2 h at room temperature. Then the embryos were incubated with primary antibody overnight at 4 °C. Next day 1X PBST washes, appropriate secondary antibody incubation overnight at 4 °C. After washing, DAPI (1µg/ml) was added for 10min followed by washing with 1X PBS and stored at -20 °C until confocal/fluorescence imaging.(Schulte-Merker et al. 1992) The mitotic phenotypes were quantified using 3D reconstruction of the confocal images using the IMARIS software.

Acridine orange staining

Acridine orange (AO) staining was performed to detect the apoptotic cells in 1dpf embryos. Embryos were dechorinated, and stained with 5mg/L AO for 1 hour in the dark followed by washing with embryo water. Then the embryos were anesthetized with tricaine and were photographed by a Zeiss AxioZoom.V16 microscope, the bright green dots in the embryos indicate apoptotic cells. The number of apoptotic cells in the head region was counted using Image J software.(Tucker and Lardelli 2007)

Skeletal preparations by Alcian blue and Alizarin red staining

Wild-type control and morphants 5-day-old larvae were fixed in 4% PFA/PBS overnight at 4^0C. The embryos were washed with 1XPBS and stored overnight in 100% methanol at -20^0C. The following staining solutions were prepared - Solution A (0.04% Alcian blue, 125mM MgCl2 in 70% ethanol) and Solution B (1.5% Alizarin Red S). 1ml of solution A and 10ul of solution B were added to the larvae and kept overnight at room temperature with constant rocking. The staining solution was removed and the larvae were washed two times with water, followed by bleach solution for 1 hour at room temperature and a gradation of Glycerol-KOH. The embryos were then stored in 50% glycerol/ 0.25% KOH for 2 hours at room temperature. The stained larvae were then imaged using a Zeiss Stemi508 stereomicroscope. For microcephaly analyses of zebrafish 5dpf larval head area was defined by the otic vesicle and the semicircle of eyes as posterior and lower boundary, respectively. The interpupillary distance (IPD) and distance between irises are also measured and quantitated using ImageJ software.(Faundes et al. 2021)

Phalloidin Staining

Embryos were dechorinated and fixed using 4% paraformaldehyde for overnight at 4°C. Embryos were washed out of 4% paraformaldehyde at least three times with Phosphate Buffered Saline-0.1% Tween20 (PBT). Prior to phalloidin staining, embryos were permeabilized for 30min at room temperature with PBS-1%Trition. Embryos were incubated in Phalloidin–Tetramethylrhodamine B isothiocyanate (cat no.P1951) at 1:500 dilution overnight at 4°C. Embryos were washed three times in PBS-0.1%Tw prior to imaging.

Pharmacological modulation of the Wnt/β-catenin signaling pathway

Zebrafish embryos were treated at shield stage with 10 µM XAV939 and 10 µM CHIR99021 dissolved in DMSO, to inhibit (XAV939) or activate (CHIR99021) Wnt/β-catenin signalling. At 24hpf the percent phenotype was calculated for all these treated groups of embryos.

RNAseq-based gene expression analysis

The total RNA was extracted from 1dpf control and *rapgef1b* depleted embryos using an RNA isolation kit (MN; 740955.50). Sequencing libraries were generated using MGIEasy RNA library prep set (MGI) according to the manufacturer's instructions. Here, 500 ng total RNA was used as starting material, and rRNA was depleted by MGIEasy rRNA depletion Kit. The rRNA-depleted samples were fragmented, reverse transcribed and the second strand was synthesized and converted to cDNA. DNA was then purified using DNA Clean Beads provided in the kit followed by end repair and A-tailing. Barcoding and adaptor ligation were performed and the samples were purified. Samples were amplified using adaptor-specific primers and quantified using a Qubit dsDNA high-sensitivity kit (ThermoScientific). Sample fragment size was determined using 4200 TapeStation (Agilent). 1pMol of the dsDNA library was denatured and circularized to make single-stranded circular DNA. DNA Nano Balls

(DNBs) were created using Rolling cycle amplification. DNBs were loaded onto patterned flowcell and sequenced using PE100 recipe on MGISEQ-2000 sequencer (MGI).

The raw sequence data from the control and *rapgef1b-depleted* embryos were evaluated for read quality status using FASTQC.(Banu et al. 2021) The RNAseq data was uploaded on Gene Expression Omnibus (GEO), accession no. GSE283261. Adapter trimming and read filtration were performed using CUTADAPT, and the filtration criteria were set to a minimum length (50bp), and a minimal quality score (Q20) cutoffs. The trimmed reads were then mapped onto the zebrafish fish reference genome (GRCz11) using STAR aligner (Banu et al. 2021) STAR was run in quant-mode, instructing the tool to generate the read counts and alignments. The differential gene expression was performed using the DESeq2 package (Love et al. 2014), assayed across the three replicates of each condition; control (WT) and *rapgef1b* knockdown (*rapgef1b* KD). Transcripts with a raw count sum of less than 10 were excluded for downstream analysis. A correlation matrix was calculated to determine the agreement of various replicates across conditions. To ensure consistency across conditions and the replicates, principal component analysis (PCA) was carried out of deseq2 normalized counts. Significantly differentially expressed transcripts were obtained by filtering for a false discovery rate (FDR) by filtering p-adjusted cutoff of $p <= 0.05$. These are then classified as upregulated and downregulated based on their respective log fold change (L.F.C) values, which is representative of their regulation states; transcripts that had a fold change greater than 1 (L.F.C>=1) were considered as up-regulated while those lesser than -1 (F.C<=-1) were deemed down-regulated. Gene ontology (GO) enrichment analysis was performed using the enrichGO module of the ClusterProfiler package to analyze the effect of these gene subsets on metabolic networks.(Yu et al. 2012)

List of abbreviations

GEFs - Guanine Nucleotide Exchange Factors

CBR - Crk binding region

ISH - *in situ* hybridization

MHB - midbrain-hindbrain boundary

HA - head area

IPD - interpupillary distance

ID - iris distance

PSM – presomitic mesoderm

Declaration of Competing Interests

The authors declare no competing interests.

Credit authorship contribution statement

TP performed the morpholino and CRISPR experiments, PCR, ISH and analyzed the data, prepared the figures, and assisted in manuscript writing. SI performed the cloning of ISH markers, ISH, immunohistochemistry, imaging, and analyzed the data. SD performed ISH, imaging, and analyzed data. RJM analyzed the transcriptome data and prepared the figure. DTS supervised the transcriptome analysis. VR and MK developed the concept. TP, VR and MK designed the experiments and interpreted the data. MK supervised and mentored the entire study, and wrote the manuscript with input from other authors.

Funding and Acknowledgments

TP and SI acknowledge CSIR, India for the research fellowship. We thank Valli Undamatla from NGS Facility, CSIR-CCMB for help in NGS sample preparation and sequencing. VR

recognizes CSIR for the award of ES scheme, 21(1089)/19/EMR-II. MK thanks the Council of Scientific and Industrial Research- Centre for Cellular and Molecular Biology (CSIR-CCMB), Govt. of India, and the Department of Science and Technology (DST), Govt. of India (DST/INSPIRE/04/2016/001436) for support and funding this research.

References:

Amacher, S. L., Draper, B. W., Summers, B. R., & Kimmel, C. B. 2002. The zebrafish T-box genes no tail and spadetail are required for development of trunk and tail mesoderm and medial floor plate. *Development* **129**: 3311–3323. https://doi.org/10.1242/dev.129.14.3311.

Asad Z, Pandey A, Babu A, Sun Y, Shevade K, Kapoor S, Ullah I, Ranjan S, Scaria V, Bajpai R, et al. 2016. Rescue of neural crest-derived phenotypes in a zebrafish CHARGE model by Sox10 downregulation. *Hum Mol Genet* **25**: 3539–3554.

Bajard L, Morelli LG, Ares S, Pécréaux J, Jülicher F, Oates AC. 2014. Wnt-regulated dynamics of positional information in zebrafish somitogenesis. *Development* **141**: 1381–1391. https://hal.science/hal-01064627.

Banu S, Srivastava S, Mohammed A, Kushawah G, Sowpati DT, Mishra RK. 2021. Tissue-specific transcriptome recovery on withdrawal from chronic alcohol exposure in zebrafish. *Alcohol* **91**: 29–38.

Bryson-Richardson RJ, Daggett DF, Cortes F, Neyt C, Keenan DG, Currie PD. 2005. Myosin heavy chain expression in zebrafish and slow muscle composition. *Dev Dyn* **233**: 1018–1022.

Buckles GR, Thorpe CJ, Ramel MC, Lekven AC. 2004. Combinatorial Wnt control of zebrafish midbrain-hindbrain boundary formation. *Mech Dev* **121**: 437–447.

Carabias A, Gómez-Hernández M, de Cima S, Rodríguez-Blázquez A, Morán-Vaquero A, González-Sáenz P, Guerrero C, de Pereda JM. 2020. Mechanisms of autoregulation of C3G, activator of the GTPase Rap1, and its catalytic deregulation in lymphomas. *Sci Signal* **13**: 1–17.

Carney TJ, Dutton KA, Greenhill E, Delfino-Machín M, Dufourcq P, Blader P, Kelsh RN. 2006. A direct role for Sox10 in specification of neural crest-derived sensory neurons.

Development **133**: 4619–4630.

Carraco G, Martins-Jesus AP, Andrade RP. 2022. The vertebrate Embryo Clock: Common players dancing to a different beat. *Front Cell Dev Biol* **10**.

Chalamalasetty RB, Garriock RJ, Dunty WC, Kennedy MW, Jailwala P, Si H, Yamaguchi TP. 2014. Mesogenin 1 is a master regulator of paraxial presomitic mesoderm differentiation. *Dev* **141**: 4285–4297.

Chapman, D. L., & Papaioannou, V. E. 1998. Three neural tubes in mouse embryos with mutations in the T-box gene Tbx6. *Nature*, **391**: 695–697. https://doi.org/10.1038/35624

Choorapoikayil S, Willems B, Ströhle P, Gajewski M. 2012. Analysis of her1 and her7 mutants reveals a spatio temporal separation of the Somite clock module. *PLoS One* **7**.

Cuesta ÁM, Palao N, Bragado P, Gutierrez-Uzquiza A, Herrera B, Sánchez A, Porras A. 2023. New and Old Key Players in Liver Cancer. *Int J Mol Sci* **24**: 1–31.

Dayma K, Ramadhas A, Sasikumar K, Radha V. 2012. Reciprocal Negative Regulation between the Guanine Nucleotide Exchange Factor C3G and β-Catenin. *Genes and Cancer* **3**: 564–577.

Delfino-Machín M, Madelaine R, Busolin G, Nikaido M, Colanesi S, Camargo-Sosa K, Law EWP, Toppo S, Blader P, Tiso N, et al. 2017. Sox10 contributes to the balance of fate choice in dorsal root ganglion progenitors. *PLoS One* **12**.

Diez del Corral R, Morales A V. 2017. The multiple roles of FGF signaling in the developing spinal cord. *Front Cell Dev Biol* **5**.

Drerup CM, Wiora HM, Topczewski J, Morris JA. 2009. Disc1 regulates foxd3 and sox10 expression, affecting neural crest migration and differentiation. *Development* **136**: 2623–2632.

Duan W, Zhang YP, Hou Z, Huang C, Zhu H, Zhang CQ, Yin Q. 2016. Novel Insights into

NeuN: from Neuronal Marker to Splicing Regulator. *Mol Neurobiol* **53**: 1637–1647.

Dutton KA. 2001. *Zebrafish sox10 mutant*. www.hgmp.mrc.ac.uk/Registered/Option/mrtrans.html.

Faundes V, Jennings MD, Crilly S, Legraie S, Withers SE, Cuvertino S, Davies SJ, Douglas AGL, Fry AE, Harrison V, et al. 2021. Impaired eIF5A function causes a Mendelian disorder that is partially rescued in model systems by spermidine. *Nat Commun* **12**: 1–14. http://dx.doi.org/10.1038/s41467-021-21053-2.

Fior R, Maxwell AA, Ma TP, Vezzaro A, Moens CB, Amacher SL, Lewis J, Saúde L. 2012. The differentiation and movement of presomitic mesoderm progenitor cells are controlled by mesogenin 1. *Dev* **139**: 4656–4665.

Foley TE, Hess B, Savory JGA, Ringuette R, Lohnes D. 2019. Role of cdx factors in early mesodermal fate decisions. *Dev* **146**.

Franke M, De la Calle-Mustienes E, Neto A, Almuedo-Castillo M, Irastorza-Azcarate I, Acemel RD, Tena JJ, Santos-Pereira JM, Gómez-Skarmeta JL. 2021. CTCF knockout in zebrafish induces alterations in regulatory landscapes and developmental gene expression. *Nat Commun* **12**. http://dx.doi.org/10.1038/s41467-021-25604-5.

Gladysheva J, Evnukova E, Kondakova E, Kulakova M, Efremov V. 2021. Neurulation in the posterior region of zebrafish, Danio rerio embryos. *J Morphol* **282**: 1437–1454.

Gogos A, Sun J, Udawela M, Gibbons A, van den Buuse M, Scarr E, Dean B. 2021. Cortical expression of the RAPGEF1 gene in schizophrenia: investigating regional differences and suicide. *Psychiatry Res* **298**: 113818. https://doi.org/10.1016/j.psychres.2021.113818.

Gou Y, Vemaraju S, Sweet EM, Kwon HJ, Riley BB. 2018. sox2 and sox3 Play unique roles in development of hair cells and neurons in the zebrafish inner ear. *Dev Biol* **435**: 73–83.

Griffin, K. J., Amacher, S. L., Kimmel, C. B., & Kimelman, D. 1998. Molecular

identification of spadetail: regulation of zebrafish trunk and tail mesoderm formation by T-box genes. *Development* **125**: 3379–3388. https://doi.org/10.1242/dev.125.17.3379

Guerrero C, Fernandez-Medarde A, Rojas JM, Font De Mora J, Esteban LM, Santos E. 1998. Transformation suppressor activity of C3G is independent of its CDC25-homology domain. *Oncogene* **16**: 613–624.

Hagey DW, Klum S, Kurtsdotter I, Zaouter C, Topcic D, Andersson O, Bergsland M, Muhr J. 2018. SOX2 regulates common and specific stem cell features in the CNS and endoderm derived organs. *PLoS Genet* **14**.

Hans S, Liu D, Westerfield M. 2004. Pax8 and Pax2a function synergistically in otic specification, downstream of the Foxi1 and Dlx3b transcription factors. *Development* **131**: 5091–5102.

Harrington MJ, Hong E, Fasanmi O, Brewster R. 2007. Cadherin-mediated adhesion regulates posterior body formation. *BMC Dev Biol* **7**.

Henry CA, Hall LA, Burr Hille M, Solnica-Krezel L, Cooper MS. 1063. *Brief Communication*.

Hofmann M, Schuster-Gossler K, Watabe-Rudolph M, Aulehla A, Herrmann BG, Gossler A. 2004. WNT signaling, in synergy with T/TBX6, controls Notch signaling by regulating Dll1 expression in the presomitic mesoderm of mouse embryos. *Genes Dev* **18**: 2712–2717.

Holley SA, Geisler R, Nü Sslein-Volhard C. 2000. *Control of her1 expression during zebrafish somitogenesis by a Delta-dependent oscillator and an independent wave-front activity*. www.genesdev.org.

Hong KW, Jin HS, Lim JE, Ryu HJ, Go MJ, Lee JY, Woo JT, Park HK, Oh B. 2009. RAPGEF1 gene variants associated with type 2 diabetes in the Korean population.

Diabetes Res Clin Pract **84**: 117–122.

Housley MP, Reischauer S, Dieu M, Raes M, Stainier DYR, Vanhollebeke B. 2014. Translational profiling through biotinylation of tagged ribosomes in zebrafish. *Dev* **141**: 3988–3993.

Hug B, Walter V, Grunwald DJ. 1997. *tbx6, a Brachyury-Related Gene Expressed by Ventral Mesendodermal Precursors in the Zebrafish Embryo*.

Iyer S, Dhiman N, Zade SP, Mukherjee S, Singla N, Kumar M. 2023. Exposure to Tetrabutylammonium Bromide Impairs Cranial Neural Crest Specification, Neurogenic Program, and Brain Morphogenesis. *ACS Chem Neurosci* **14**: 1785–1798.

Jeong KH, Jeong JY, Lee HO, Choi E, Lee H. 2010. Inhibition of Plk1 induces mitotic infidelity and embryonic growth defects in developing zebrafish embryos. *Dev Biol* **345**: 34–48.

Jin Y, Zheng S, Fu Z. 2011. Embryonic exposure to cypermethrin induces apoptosis and immunotoxicity in zebrafish (Danio rerio). *Fish Shellfish Immunol* **30**: 1049–1054. http://dx.doi.org/10.1016/j.fsi.2011.02.001.

Kim S-H, Yamamoto A, Bouwmeester T, Agius E, De Robertis EM. *The role of Paraxial Protocadherin in selective adhesion and cell movements of the mesoderm during Xenopus gastrulation*. https://www.hhmi.ucla.edu/derobertis/EDR_MS/papc_page/papc.html.

Kimmel CB, Ballard WW, Kimmel SR, Ullmann B, Schilling TF. 1995. Stages of embryonic development of the zebrafish. *Dev Dyn* **203**: 253–310.

Kinney BA, Al Anber A, Row RH, Tseng YJ, Weidmann MD, Knaut H, Martin BL. 2020. Sox2 and Canonical Wnt Signaling Interact to Activate a Developmental Checkpoint Coordinating Morphogenesis with Mesoderm Fate Acquisition. *Cell Rep* **33**.

Li N, Zhou P, Yang M, Fang X, Krämer N, Mughal TA, Abbasi AA, Yang Y, Kaindl AM,

Hu H. 2021. Zebrafish modeling mimics developmental phenotype of patients with RAPGEF1 mutation. *Clin Genet* **100**: 144–155.

Liu G, Ito T, Kijima Y, Yoshitake K, Asakawa S, Watabe S, Kinoshita S. 2022. Zebrafish Danio rerio myotomal muscle structure and growth from a spatial transcriptomics perspective. *Genomics* **114**: 110477. https://doi.org/10.1016/j.ygeno.2022.110477.

Love MI, Huber W, Anders S. 2014. Moderated estimation of fold change and dispersion for RNA-seq data with DESeq2. *Genome Biol* **15**: 1–21.

Lusk S, Kwan KM. 2022. Pax2a, but not pax2b, influences cell survival and periocular mesenchyme localization to facilitate zebrafish optic fissure closure. *Dev Dyn* **251**: 625–644.

Mackereth MD, Kwak SJ, Fritz A, Riley BB. 2005. Zebrafish pax8 is required for otic placode induction and plays a redundant role with Pax2 genes in the maintenance of the otic placode. *Development* **132**: 371–382.

Manzano S, Gutierrez-uzquiza A, Bragado P, Cuesta AM, Guerrero C, Porras A. 2021. C3G protein, a new player in glioblastoma. *Int J Mol Sci* **22**.

Marada S, Truong A, Ogden SK. 2016. The small GTPase Rap1 is a modulator of Hedgehog signaling. *Dev Biol* **409**: 84–94.

McCarroll, M. N., Lewis, Z. R., Culbertson, M. D., Martin, B. L., Kimelman, D., & Nechiporuk, A. V. 2012. Graded levels of Pax2a and Pax8 regulate cell differentiation during sensory placode formation. *Development* **139**: 2740–2750. https://doi.org/10.1242/dev.076075

Ohba, Y., Ikuta, K., Ogura, A., Matsuda, J., Mochizuki, N., Nagashima, K., Kurokawa, K., Mayer, B. J., Maki, K., Miyazaki, J., & Matsuda, M. 2001. Requirement for C3G-dependent Rap1 activation for cell adhesion and embryogenesis. *The EMBO journal*, **20**: 3333–3341. https://doi.org/10.1093/emboj/20.13.3333

Maves L, Kimmel CB. 2005. Dynamic and sequential patterning of the zebrafish posterior hindbrain by retinoic acid. *Dev Biol* **285**: 593–605.

Nagao Y, Takada H, Miyadai M, Adachi T, Seki R, Kamei Y, Hara I, Taniguchi Y, Naruse K, Hibi M, et al. 2018. Distinct interactions of Sox5 and Sox10 in fate specification of pigment cells in medaka and zebrafish. *PLoS Genet* **14**.

Nayak SC, Radha V. 2020. C3G localizes to the mother centriole in a cenexin-dependent manner and regulates centrosome duplication and primary cilium length. *J Cell Sci* **133**.

Oxtoby E, Jowett T. 1993. Cloning of the zebrafish krox-20 gene (krx-20) and its expression during hindbrain development. *Nucleic Acids Res* **21**: 1087–1095.

Pownall ME, Gustafsson MK, Emerson CP. 2002. Myogenic regulatory factors and the specification of muscle progenitors in vertebrate embryos. *Annu Rev Cell Dev Biol* **18**: 747–783.

Radha V, Mitra A, Dayma K, Sasikumar K. 2011a. Signalling to actin: Role of C3G, a multitasking guanine-nucleotide- exchange factor. *Biosci Rep* **31**: 231–244.

Radha V, Mitra A, Dayma K, Sasikumar K. 2011b. Signalling to actin: role of C3G, a multitasking guanine-nucleotide-exchange factor. *Biosci Rep*. www.bioscirep.org.

Radha V, Rajanna A, Swarup G. 2004. Phosphorylated guanine nucleotide exchange factor C3G, induced by pervanadate and Src family kinases localizes to the Golgi and subcortical actin cytoskeleton. *BMC Cell Biol* **5**: 1–15.

Rocha M, Kushkowski E, Schnirman R, Booth C, Singh N, Beadell A, Prince VE. 2021. Zebrafish Cdx4 regulates neural crest cell specification and migratory behaviors in the posterior body. *Dev Biol* **480**: 25–38.

Ryan N, Ormond C, Chang YC, Contreras J, Raventos H, Gill M, Heron E, Mathews CA, Corvin A. 2022. Identity-by-descent analysis of a large Tourette's syndrome pedigree from Costa Rica implicates genes involved in neuronal development and signal

transduction. *Mol Psychiatry* **27**: 5020–5027.

Samuelsson J, Alonso S, Ruiz-Larroya T, Cheung TH, Wong YF, Perucho M. 2011. Frequent somatic demethylation of RAPGEF1/C3G intronic sequences in gastrointestinal and gynecological cancer. *Int J Oncol* **38**: 1575–1577.

Schröter C, Ares S, Morelli LG, Isakova A, Hens K, Soroldoni D, Gajewski M, Jülicher F, Maerkl SJ, Deplancke B, et al. 2012. Topology and dynamics of the zebrafish segmentation clock core circuit. *PLoS Biol* **10**: 11.

Schulte-Merker S, Ho RK, Herrmann BG, Nüsslein-Volhard C. 1992. The protein product of the zebrafish homologue of the mouse T gene is expressed in nuclei of the germ ring and the notochord of the early embryo. *Development* **116**: 1021–1032.

Seitanidou T, Schneider-Maunoury S, Desmarquet C, Wilkinson DG, Charnay P. 1997. Krox-20 is a key regulator of rhombomere-specific gene expression in the developing hindbrain. *Mech Dev* **65**: 31–42.

Sequera C, Manzano S, Guerrero C, Porras A. 2018. How Rap and its GEFs control liver physiology and cancer development. C3G alterations in human hepatocarcinoma. *Hepatic Oncol* **5**: HEP05.

Shah B, Lutter D, Bochenek ML, Kato K, Tsytsyura Y, Glyvuk N, Sakakibara A, Klingauf J, Adams RH, Püschel AW. 2016. C3G/Rapgef1 is required in multipolar neurons for the transition to a bipolar morphology during cortical development. *PLoS One* **11**.

Shakyawar DK, Dayma K, Ramadhas A, Varalakshmi C, Radha V. 2017. C3G shows regulated nucleocytoplasmic exchange and represses histone modifcations associated with euchromatin. *Mol Biol Cell* **28**: 984–995.

Shimizu T, Bae YK, Muraoka O, Hibi M. 2005. Interaction of Wnt and caudal-related genes in zebrafish posterior body formation. *Dev Biol* **279**: 125–141.

Shirinian M, Grabbe C, Popovic M, Varshney G, Hugosson F, Bos H, Rehmann H, Palmer

RH. 2010. The rap1 guanine nucleotide exchange factor C3G is required for preservation of larval muscle integrity in Drosophila melanogaster. *PLoS One* **5**.

Shivakrupa, Singh R, Swarup G. 1999. Identification of a novel splice variant of C3G which shows tissue- specific expression. *DNA Cell Biol* **18**: 701–708.

Sieger D, Ackermann B, Winkler C, Tautz D, Gajewski M. 2006. her1 and her13.2 are jointly required for somitic border specification along the entire axis of the fish embryo. *Dev Biol* **293**: 242–251.

Sriram D, Chintala R, Parthasaradhi BVV, Nayak SC, Mariappan I, Radha V. 2020. Expression of a novel brain specific isoform of C3G is regulated during development. *Sci Rep* **10**.

Sriram D, Dayma K, Devi AS, Raghawan AK, Rawat S, Radha V. 2021. Complex formation and reciprocal regulation between GSK3β and C3G. *Biochim Biophys Acta - Mol Cell Res* **1868**.

Szeto DP, Kimelman D. 2006. The regulation of mesodermal progenitor cell commitment to somitogenesis subdivides the zebrafish body musculature into distinct domains. *Genes Dev* **20**: 1923–1932.

Tan AL, Christensen SE, Baker AK, Riley BB. 2023. Fgf, Hh, and pax2a differentially regulate expression of pax5 and pou3f3b in vestibular and auditory maculae in the zebrafish otic vesicle. *Dev Dyn* **252**: 1269–1279.

Thierion E, Le Men J, Collombet S, Hernandez C, Coulpier F, Torbey P, Thomas-Chollier M, Noordermeer D, Charnay P, Gilardi-Hebenstreit P. 2017. Krox20 hindbrain regulation incorporates multiple modes of cooperation between cis-acting elements. *PLoS Genet* **13**: 1–18.

Trofka A, Schwendinger-Schreck J, Brend T, Pontius W, Emonet T, Holley SA. 2012. The Her7 node modulates the network topology of the zebrafish segmentation clock via

sequestration of the Hes6 hub. *Development* **139**: 940–947.

Tucker B, Lardelli M. 2007. A rapid apoptosis assay measuring relative acridine orange fluorescence in zebrafish embryos. *Zebrafish* **4**: 113–116.

Verma, A., Goel, A., Koner, N., Gunasekaran, G., & Radha, V. 2024. Development and tissue specific expression of RAPGEF1 (C3G) transcripts having exons encoding disordered segments with predicted regulatory function. *Molecular biology reports*, *51*(1), 907. https://doi.org/10.1007/s11033-024-09845-3

Vishnu V V, Muralikrishna B, Verma A, Chavan Nayak S, Divya &, Sowpati T, Radha V, Chandra Shekar & P. 2015. C3G Regulates STAT3, ERK, Adhesion Signaling, and Is Essential for Differentiation of Embryonic Stem Cells. https://doi.org/10.1007/s12015-021-10136-8.

Voss AK, Britto JM, Dixon MP, Sheikh BN, Collin C, Tan SS, Thomas T. 2008. C3G regulates cortical neuron migration, preplate splitting and radial glial cell attachment. *Development* **135**: 2139–2149.

Voss AK, Gruss P, Thomas T. 2003. The guanine nucleotide exchange factor C3G is necessary for the formation of focal adhesions and vascular maturation. *Development* **130**: 355–367.

Voss AK, Krebs DL, Thomas T. 2006. C3G regulates the size of the cerebral cortex neural precursor population. *EMBO J* **25**: 3652–3663.

Wang J, Thomas HR, Li Z, Yeo NC, Scott HE, Dang N, Hossain MI, Andrabi SA, Parant JM. 2021. Puma, noxa, p53, and p63 differentially mediate stress pathway induced apoptosis. *Cell Death Dis* **12**. http://dx.doi.org/10.1038/s41419-021-03902-6.

Weinberg, E. S., Allende, M. L., Kelly, C. S., Abdelhamid, A., Murakami, T., Andermann, P., Doerre, O. G., Grunwald, D. J., & Riggleman, B. 1996. Developmental regulation of zebrafish MyoD in wild-type, no tail and spadetail embryos. *Development* **122**: 271–

280. https://doi.org/10.1242/dev.122.1.271

Weiser DC, Row RH, Kimelman D. 2009. Rho-regulated Myosin phosphatase establishes the level of protrusive activity required for cell movements during zebrafish gastrulation. *Development* **136**: 2375–2384.

Wittler L, Shin EH, Grote P, Kispert A, Beckers A, Gossler A, Werber M, Herrmann BG. 2007. Expression of Msgn1 in the presomitic mesoderm is controlled by synergism of WNT signalling and Tbx6. *EMBO Rep* **8**: 784–789.

Won M, Lee S, Choi S, Ro H, Kim KJ, Kim JH, Kim KE, Kim KK. 2016. Identification and characterization of the RNA-binding protein Rbfox3 in zebrafish embryo. *Biochem Biophys Res Commun* **472**: 373–378.

Yabe T, Takada S. 2012. Mesogenin causes embryonic mesoderm progenitors to differentiate during development of zebrafish tail somites. *Dev Biol* **370**: 213–222.

Yang DC, Tsai CC, Liao YF, Fu HC, Tsay HJ, Huang TF, Chen YH, Hung SC. 2011. Twist controls skeletal development and dorsoventral patterning by regulating runx2 in zebrafish. *PLoS One* **6**.

Yeo GH, Cheah FSH, Jabs EW, Chong SS. 2007. Zebrafish twist1 is expressed in craniofacial, vertebral, and renal precursors. *Dev Genes Evol* **217**: 783–789.

Yu G, Wang LG, Han Y, He QY. 2012. ClusterProfiler: An R package for comparing biological themes among gene clusters. *Omi A J Integr Biol* **16**: 284–287.

Zhai B, Huo H, Liao K. 2001. C3G, a guanine nucleotide exchange factor bound to adapter molecule c-Crk, has two alternative splicing forms. *Biochem Biophys Res Commun* **286**: 61–66.

Legends

Figure 1: Expression profile of *rapgef1* and its isoforms during embryogenesis and adult zebrafish tissues

A: Schematic illustration showing the protein domains of zRAPGEF1a and zRAPGEF1b, triangle (orange) indicates hotspot for additional exons in CBR region. Numbers indicate total amino acids and the position of insertion of additional amino acids in the alternate isoforms. B: Schematic representation of *rapgef1a* and *1b* 5' end with the primer positions (black arrows) and the exon numbers. RT-PCR analysis of *rapgef1a* and *1b* transcripts in different developmental stages. Zebrafish *rpl7* (*ribosomal protein L 7*) was the loading control. NTC represents no template control. C: Whole-mount RNA *in situ* hybridization showing *rapgef1b* expression during early development. Scale bars, 200µm. D: Western blot showing Rapgef1 levels during embryonic development. β-Tubulin and Gapdh were used as the loading controls. E: Schematic representation of *rapgef1a* and *b* exons showing predicted alternately spliced transcripts for *rapgef1a* and *1b* with nucleotide ID (https://www.ncbi.nlm.nih.gov/nuccore). Locations of isoform-specific primers (black arrows) are shown that give products of different lengths based on the presence or absence of additional exons in alternately spliced isoforms. F: RT-PCR analysis of *rapgef1* transcripts in different developmental stages using *rapgef1a* and *1b* isoform-specific primers. β actin was used as the loading control. G: Isoform-specific amplification of *rapgef1a* and *1b* transcripts in adult tissues (brain, heart, liver, ovary, fin, muscle). Zebrafish *rpl7* was used as the loading control. NTC represents no template control.

Figure 2: *Rapgef1b* is required for brain and anteroposterior axis development

A: Schematic representation of *rapgef1b* knockdown and knockout strategies by morpholino and CRISPR-Cas9-based approaches respectively. The morpholino binds to the translation

start site, abrogating protein synthesis. sgRNA was designed to generate a deletion of 366bp between exons 3 and 4. B: Gross morphological analysis of *rapgef1b* depleted embryos by morpholino and CRISPR strategies in comparison to control embryos at 1dpf showing midbrain-hindbrain boundary (red asterisk) and body axis defects (red arrow). The boxed areas show the magnified images of defects in midbrain-hindbrain defects (red asterisk) and body axis defects (red arrow). Scale bars, 500µm. C: Upper panel showing Rapgef1 levels by western blot in *rapgef1b* morpholino injected morphants. β-Tubulin was used as the loading control. The lower panel shows PCR-based analysis to validate the exonic deletion in CRISPR mutants. D: Quantification showing percent phenotype of morphants in rescue experiment. Data are shown as mean ± SEM, n=3 for each experiment. E: Rescue experiments showing the functional equivalence of human Rapgef1 as a *rapgef1b* ortholog in zebrafish embryos.

Figure 3: *Rapgef1b* is essential for cranial neural crest specification and maintenance of head size

Gene expression analysis by *in situ* hybridization in control and *rapgef1b* morphants/ mutants at 1dpf. A: *Twist1a* expression (red asterisk) in control and *rapgef1b* morphants/ mutants. B: Expression of *sox10* in *rapgef1b* morphants, mutants (red arrow), and rescue embryos (red arrowhead). Scale bars, 200µm. C: *Pax2a* expression in *rapgef1b* morphants/ mutants showing expression in the optic vesicle, midbrain-hindbrain boundary (red asterisk, inset), and otic vesicle (inset). D: Expression of *sox2* in the neural tube of *rapgef1b* morphants (red arrow). Scale bars, 200µm. E: Control and *rapgef1b* morphants showing post-mitotic neuronal marker neuN (white asterisk). Scale bars, 200µm. F: Skeletal preparations of *rapgef1b* morphants (red asterisk, inset) indicating bone and cartilage staining using Alizarin red S and Alcian blue respectively. Scale bars, 500µm. G: Quantification of microcephaly

features – head area (HA), interpupillary distance (IPD), and iris distance (ID) in *rapgef1b* morphants. All data are shown as mean ± SEM. *p<0.05, **p<0.01, ***p<0.001. n=3 for each experiment. H: Sum projection confocal images of 256 cell stage control and *rapgef1b* morphants embryos showing centrosomal staining by γ tubulin (green) and DNA (blue/DAPI). Quantification of spindle length (red dotted line), spindle pole (white asterisk), and chromosome congression defects in the *rapgef1b* morphants as compared to control. Scale bars, 50µm. All data are shown as mean ± SEM. *p<0.05, **p<0.01, ***p<0.001. n=3 for each experiment.

Figure 4: Comparative transcriptome and differential gene expression analysis indicating the role of *rapgef1b* in paraxial mesoderm differentiation

A: Volcano plot of the differentially expressed genes (DEGs) in control and *rapgef1b* morphants. Red dots represent DEGs with fold change (>1 or < -1) with p-value <0.05. Green dots represent genes that are significant with fold change (>1 or < -1) with a p-value >0.05. Blue dots represent genes with insignificant fold changes with p-value <0.05. Black dots represent the genes that show insignificant levels of DEGs expression by standards of p-value and log fold change. B: Dot plot representing the gene ontology (GO) analysis of genes upregulated in the *rapgef1b* morphants. C: Heatmap of differentially expressed genes (DEGs) in control and *rapgef1b* morphants. The colors are mapped to z-score normalized values of the log fold change across each gene set. D: Validation by qPCR of *msgn1* and *tbx16* upon *rapgef1b* depletion. E: Validation by qPCR of *bbc3* upon *rapgef1b* depletion. F: Validation by qPCR of *myhc4*, *myoz1b*, and *pavlb1* upon *rapgef1b* depletion. G: Validation by qPCR of *her13* on *rapgef1b* depletion. All data are shown as mean ± SEM. *p<0.05, **p<0.01, ***p<0.001. n=3 for each experiment.

Figure 5: *Rapgef1b* depletion results in defective somite formation and deregulation of genes involved in presomitic mesoderm specification

A: Phalloidin staining in 1dpf control and morphant embryos. Inset shows the organization of F actin muscle fibers. B: *myoD1* expression at 1dpf showing somite architecture (red arrowhead, red dotted line in inset) in morphants and rescue embryos Scale bars, 200µm. C: *Tbxta* expression in the notochord and tailbud (red arrowhead) of *rapegf1b* morphants at 1dpf. Scale bars, 200µm. D: Bright field images of control and *rapgef1b* morphants at the 6 somite stage (red arrowhead). E: *myoD1* expression in control and morphants at 6 somite stage (red asterisk) and bud stage (red arrow). F: *tbxta* gene expression at bud stage (red arrow), and somite stage (red arrow). Scale bars, 200µm. G: Expression of *her1* in control and *rapgef1b* morphants in anterior somites (red asterisk) at the 6 somite stage and tail PSM (red arrow, red asterisk) at the 18 somite stage. H: Expression of *her7* in early somitogenesis in control and *rapgef1b* morphants showing reduced expression in anterior somites (red arrow). I: *Papc* expression pattern in control and morphants showing reduced expression in anterior somites (red arrowhead, red asterisk), PSM (red arrow) at the 6 somite stage, and PSM (red arrowhead) at the 18 somite stage. J: *Fgf8* expression pattern in control and morphants showing midbrain-hindbrain boundary (red asterisk) at the bud stage and in the head (double red asterisk), somites (red arrowhead), and tailbud (red arrow) at 14 somite stage.

Figure 6: *Rapgef1b* functions by modulating Wnt/β catenin signaling during early embryonic development

A: Gene expression patterns and relative transcript levels of *cdx4* (red asterisk) and *tbx6* (red arrow) in *rapgef1b* morphants compared to control. Data are shown as mean ± SEM, *p<0.05, **p<0.01, ***p<0.001. n=3 for each experiment. Scale bars, 200µm. B: Sum

projection of confocal images of 256 cell stage control and *rapgef1b* morphants embryos showing β-catenin (white asterisk) during interphase (upper panel) and mitosis (lower panel). Scale bars, 50µm. C. Western blotting analysis showing Rapgef1, Gsk3β/phospho Gsk3β levels, and β-catenin/phospho β-catenin levels in control and *rapgef1b* morphants. β-Tubulin and Gapdh were used as the loading controls. D: Relative expression of Wnt target genes – *axin2*, *lef1* and *cyclin D1* in control and *rapgef1b* morphants. Data are shown as mean ± SEM, *p<0.05, **p<0.01, ***p<0.001. n=3 for each experiment. E: Quantification showing percent phenotype of morphants when treated with Wnt activator and Wnt inhibitor. Data are shown as mean ± SEM, n=3 for each experiment.

Fig. 7: Proposed model showing developmental functions of *rapgef1b* in early embryonic mitoses, neural crest development, mesoderm specification, and patterning.

Figure S1: Isoform-specific expression of *rapgef1* in the brain and adult zebrafish tissues

A: RT-PCR analysis of *rapgef1* transcripts in adult zebrafish tissues using N-ter primers for *rapgef1a* and *rapgef1b*. B: Western blot showing Rapgef1 protein levels in the heart, liver, and brain of adult zebrafish. β-Tubulin and β-Actin were used as the loading controls. C: RT-PCR analysis of *rapgef1a* and *1b* transcripts at different larval head and juvenile stages brain. D: Expression analysis of *rapgef1b* and its brain-specific isoform by *in situ* hybridization and cryosectioning in 3dpf larvae showing diencephalon (double red asterisk), ganglion cell layer of the eye (red arrowhead) and rods and cones (red arrow). Scale bars, 50µm.

Figure S2: Rapgef1b depletion results in developmental defects and low larval survival

A: Snapshot of sequencing analysis highlighting site for sgRNA in WT and *rapgef1b* knockout embryos. B: Percent phenotype of *rapgef1b* morphants in different concentrations of morpholino as compared to stage-matched control. All data are shown as mean ± SEM. n= 3 for all experiments. C: Percent survival of *rapgef1b* morphants over time across morpholino concentrations. D: Gross morphological analysis of *rapgef1b* morphants over larval stages to control.

Figure S3: Rapgef1b is essential for neural progenitor survival and spindle pole integrity

A: Cell death analysis in the *rapgef1b* morphants by acridine orange staining. Acridine orange positive cells (white asterisk) shown in the head. Scale bars, 200µm. Quantitation for number of acridine orange positive cells in the head is shown. All data are shown as mean ± SEM. n= 3 for all experiments. B: Relative expression of *egr2b* in *rapgef1b* morphants. Data are shown as mean ± SEM, *p<0.05, **p<0.01, ***p<0.001. n=3 for each experiment. C: Sum projection confocal images of 256 cell stage control and *rapgef1b* morphants embryos showing DNA (DAPI, blue) and centrin3 (green). Western blot analysis to show Centrin 3 depletion in morphants embryos. Scale bars, 50µm. D: Quantification of *plk1* transcripts in control and *rapgef1b* morphants. All data are shown as mean ± SEM. *p<0.05, **p<0.01, ***p<0.001. n=3 for each experiment.

Figure S4: Differential gene expression analysis between control and *rapgef1b* morphants

A: Principal component analysis (PCA) RNA-seq data, PC1 represents 70% variance, while PC2 represents 12% variance. B: Pearson correlation between samples and across replicates; a correlation coefficient (R^2) close to 1 indicates a higher relatedness while -1 indicates unrelatedness. C: Heatmap representing differential expression patterns of 497 genes identified with a false discovery rate (FDR) of 0.05 (Q <= 0.05) across WT control and *rapgef1b* KD samples (76 upregulated and 106 downregulated genes). The colours are mapped to z-score normalized values of the log fold change across each gene set. D: Dot plot representing the gene ontology (GO) analysis of downregulated differentially expressed genes.

Prasad_Fig1

A

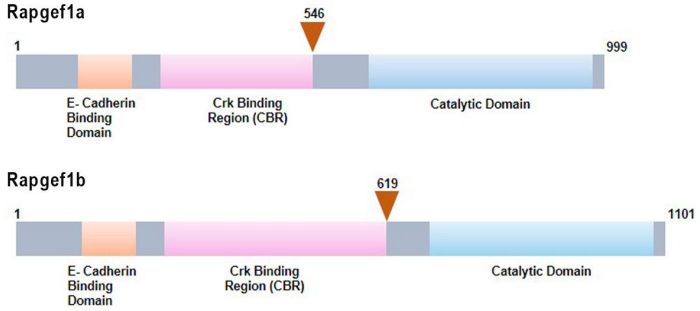

B

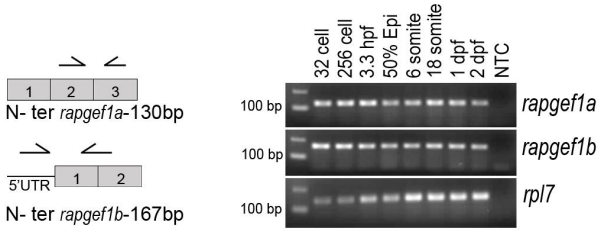

C

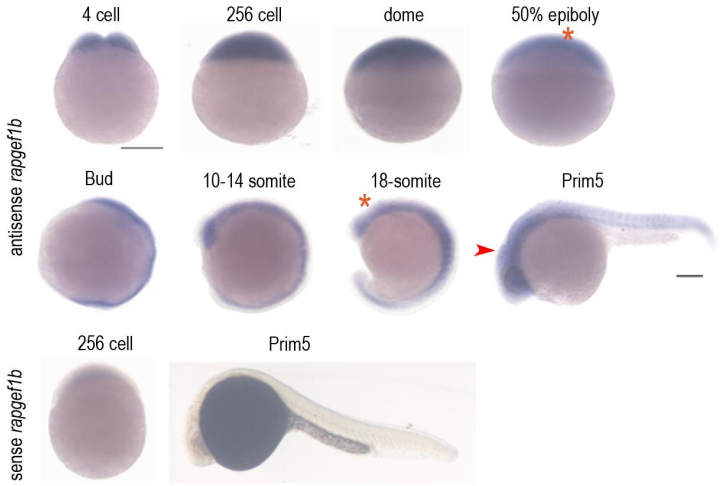

D

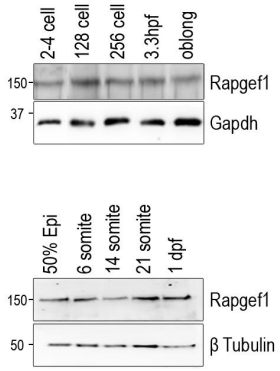

E

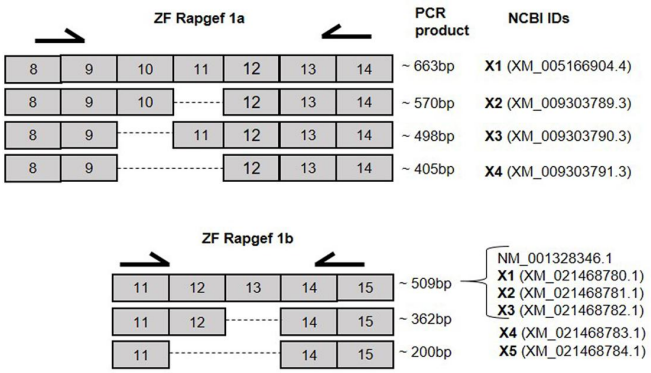

F

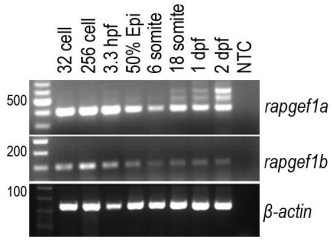

G

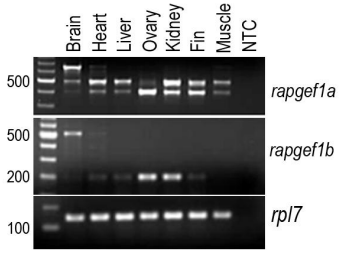

Prasad_Fig2

A

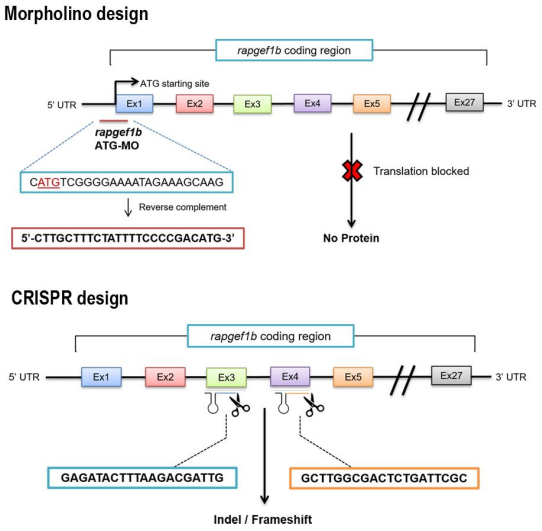

B

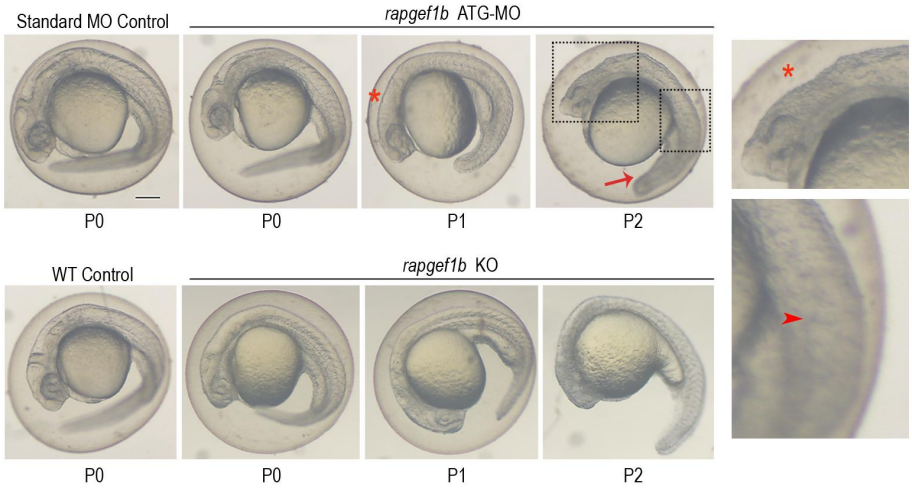

C

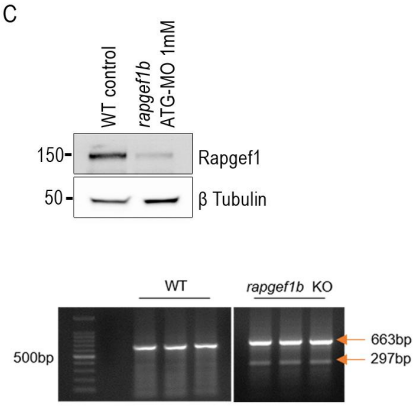

D

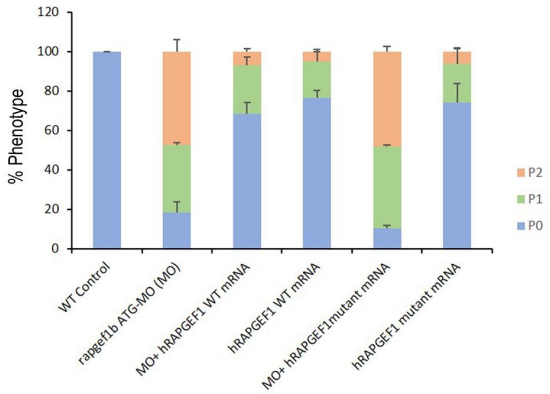

E

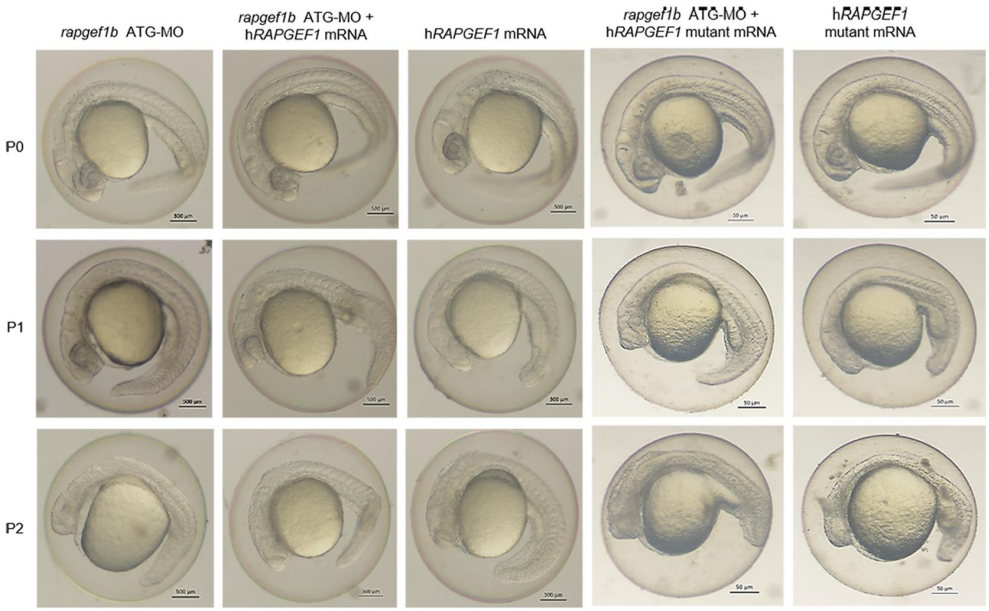

Prasad_Fig3

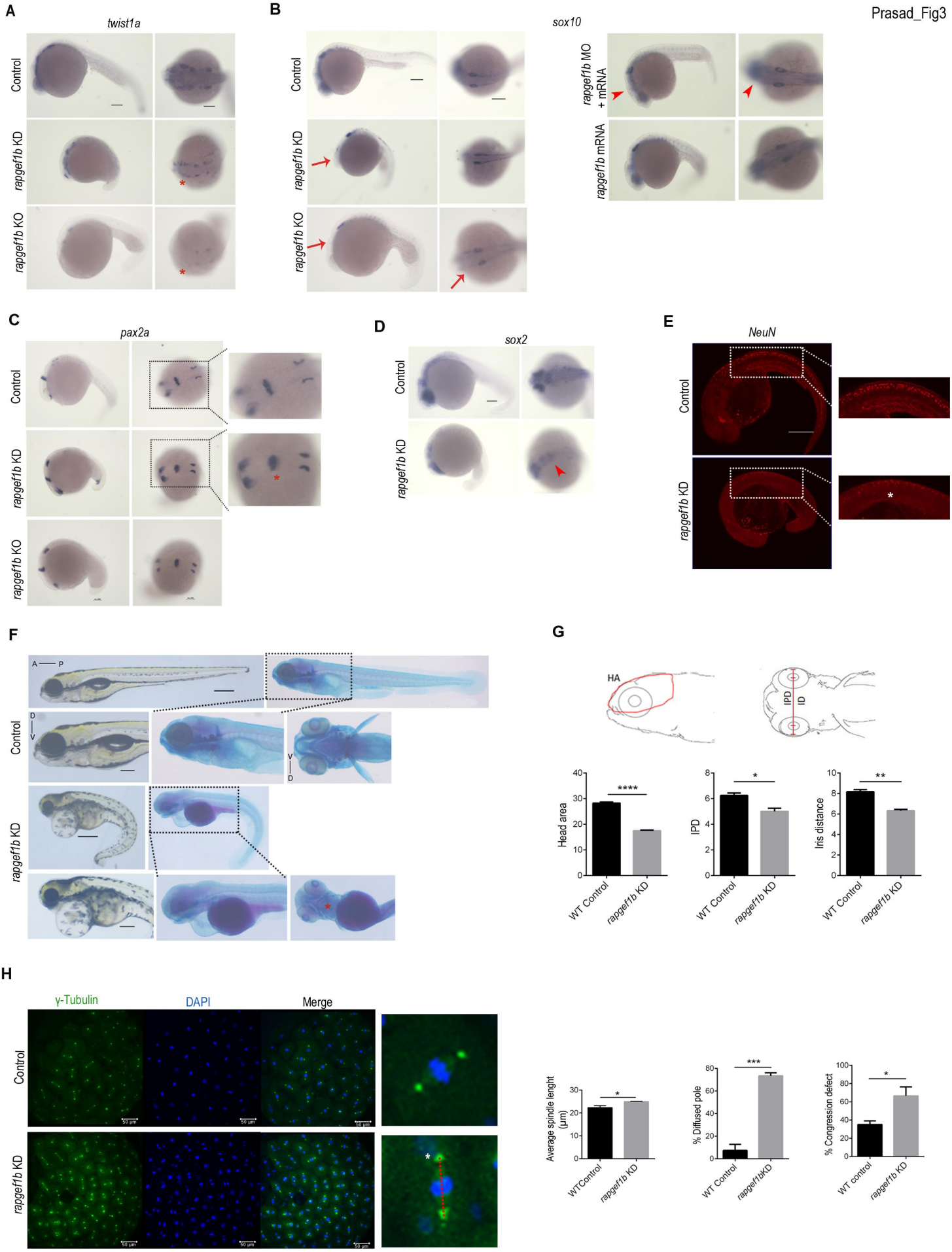
A
twist1a
Control
rapgef1b KD
rapgef1b KO
B
sox10
Control
rapgef1b KD
rapgef1b KO
rapgef1b MO + mRNA
rapgef1b mRNA
C
pax2a
Control
rapgef1b KD
rapgef1b KO
D
sox2
Control
rapgef1b KD
E
NeuN
Control
rapgef1b KD
F
A
P
Control
D
V
rapgef1b KD
G
HA
IPD
ID
Head area
IPD
Iris distance
WT Control
rapgef1b KD
H
γ-Tubulin
DAPI
Merge
Control
rapgef1b KD
Average spindle lenght (µm)
% Diffused pole
% Congression defect
WTControl
WT Control
WT control

Prasad_Fig4

A

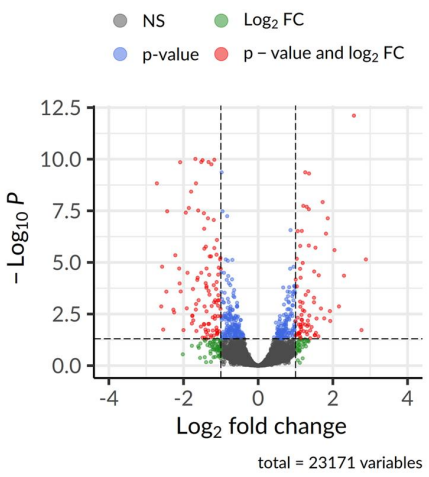

B

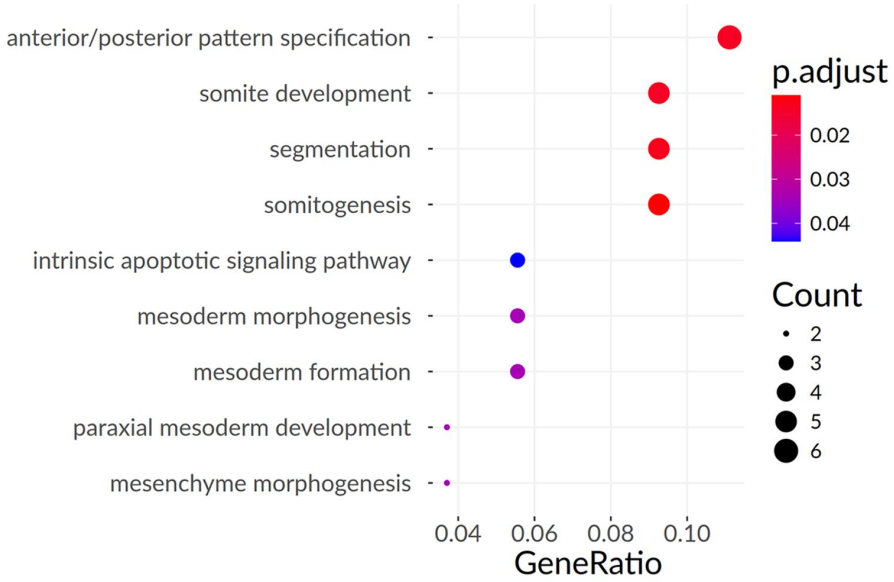

C

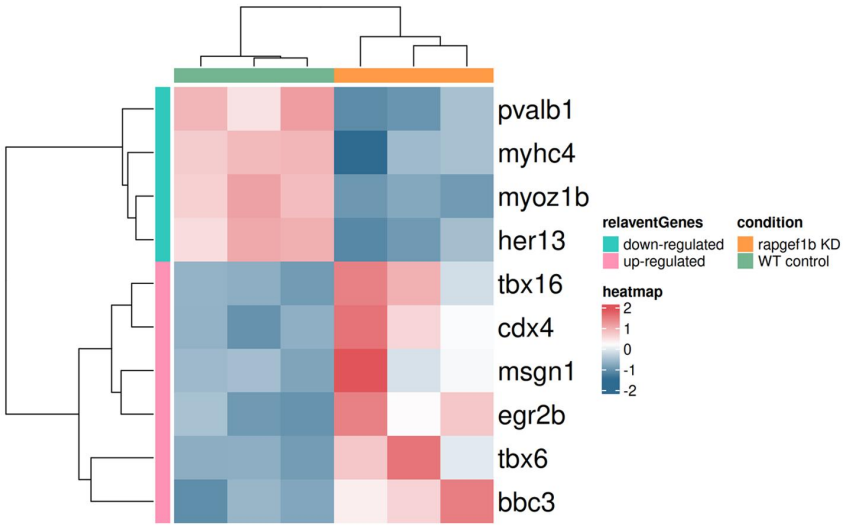

D

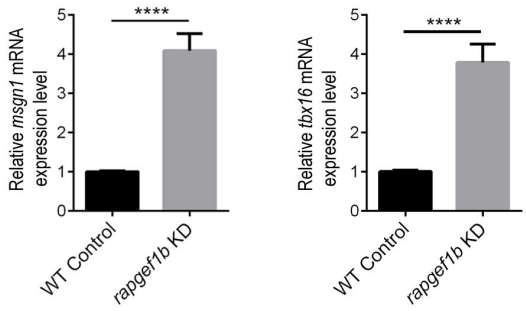

E

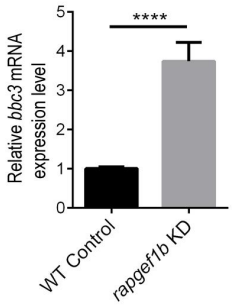

F

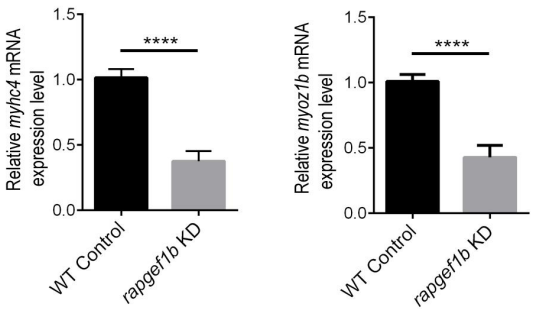

G

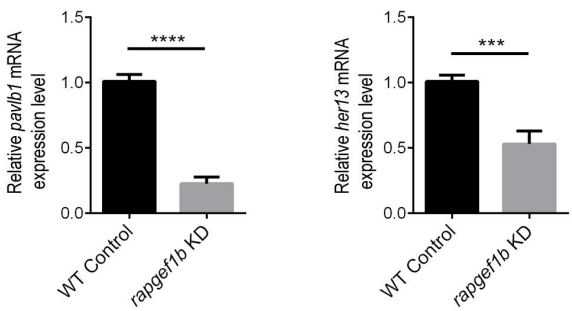

Prasad_Fig5

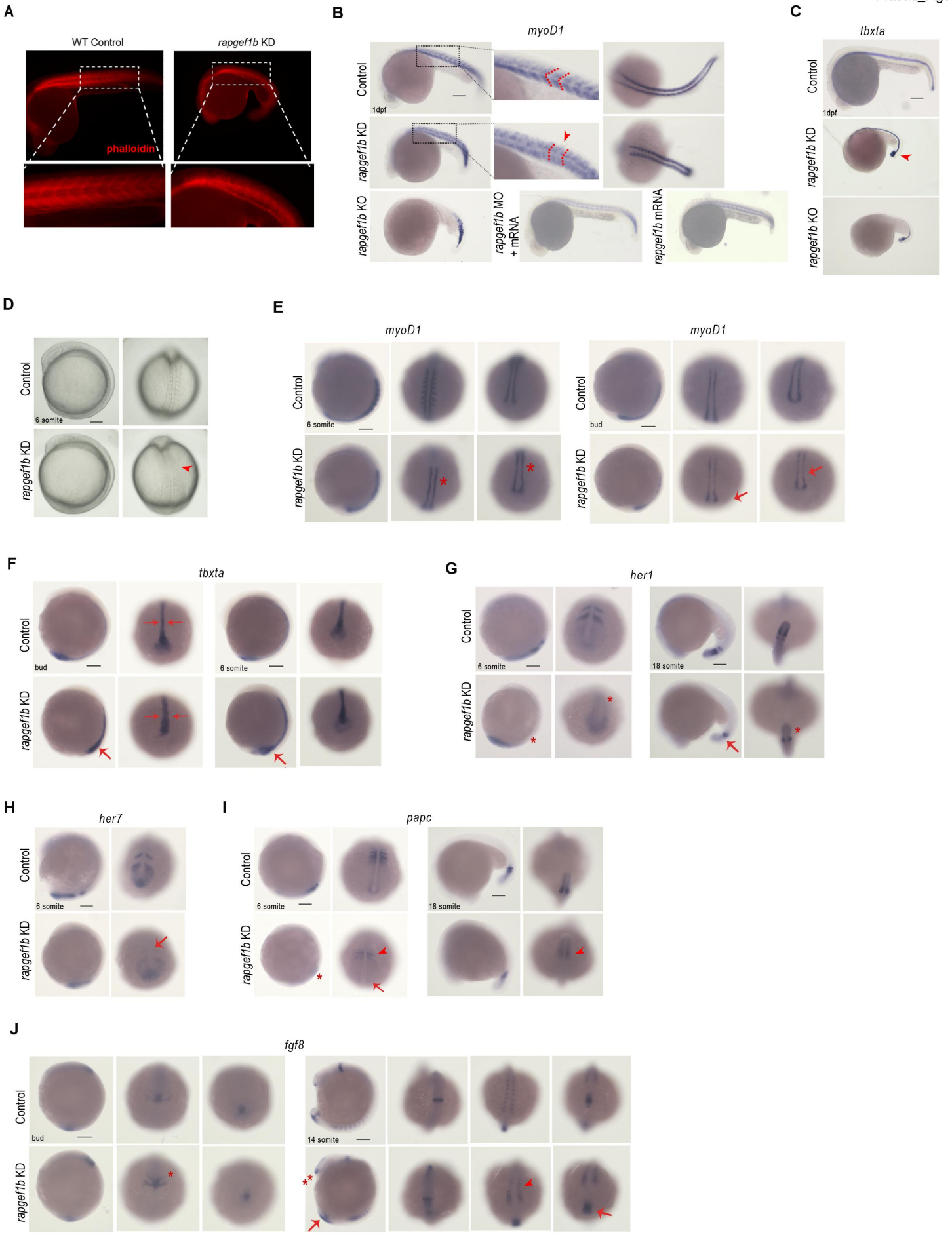
A
WT Control
rapgef1b KD
phalloidin
B
myoD1
Control
1dpf
rapgef1b KD
rapgef1b KO
rapgef1b MO + mRNA
rapgef1b mRNA
C
tbxta
Control
1dpf
rapgef1b KD
rapgef1b KO
D
Control
6 somite
rapgef1b KD
E
myoD1
Control
6 somite
rapgef1b KD
myoD1
Control
bud
rapgef1b KD
F
tbxta
Control
bud
6 somite
rapgef1b KD
G
her1
Control
6 somite
18 somite
rapgef1b KD
H
her7
Control
6 somite
rapgef1b KD
I
papc
Control
6 somite
18 somite
rapgef1b KD
J
fgf8
Control
bud
14 somite
rapgef1b KD

Prasad_Fig6

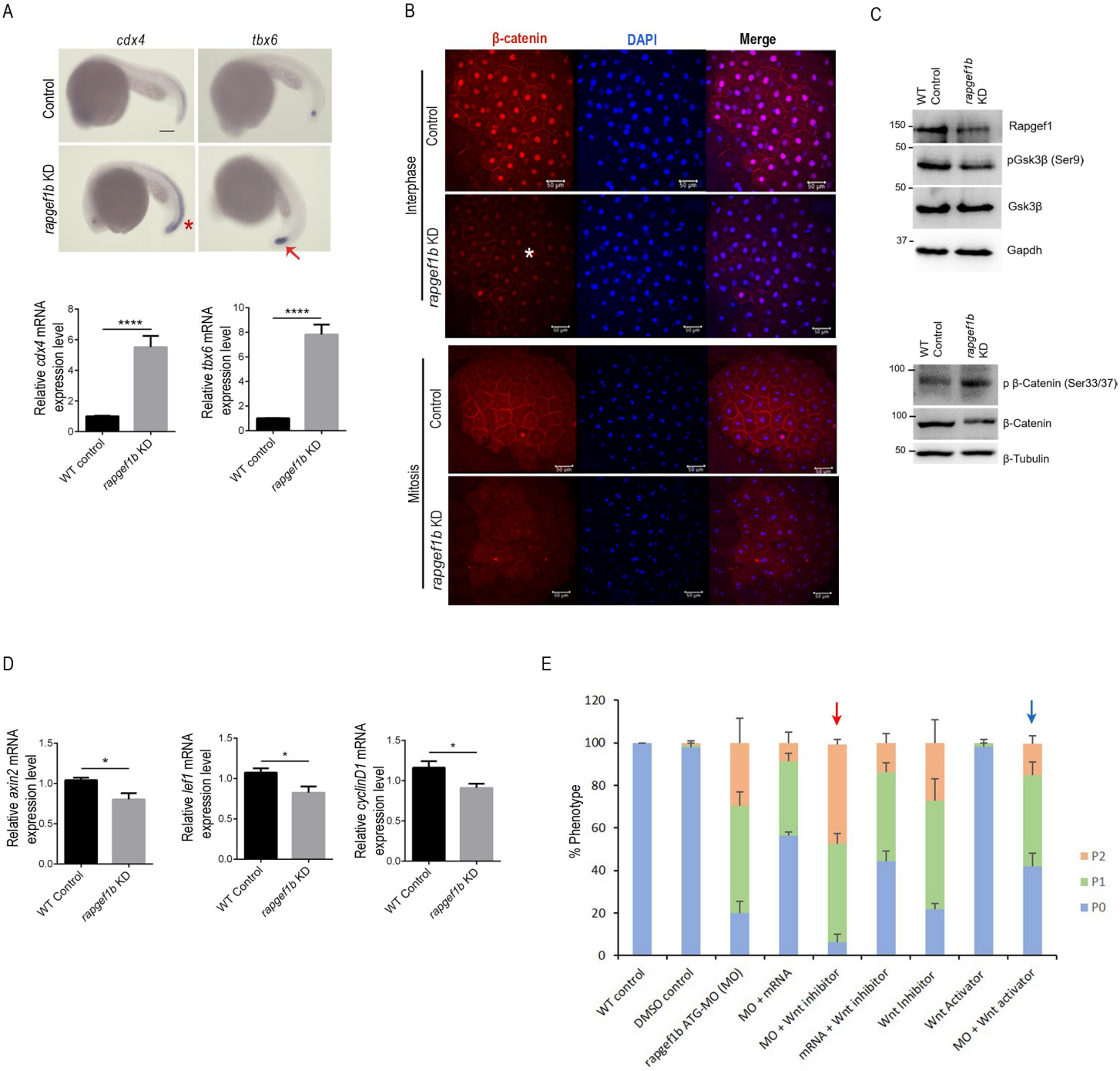
A
cdx4
tbx6
Control
rapgef1b KD
Relative cdx4 mRNA expression level
Relative tbx6 mRNA expression level
****
WT control
rapgef1b KD
B
β-catenin
DAPI
Merge
Interphase
Mitosis
Control
rapgef1b KD
C
WT Control
rapgef1b KD
Rapgef1
pGsk3β (Ser9)
Gsk3β
Gapdh
p β-Catenin (Ser33/37)
β-Catenin
β-Tubulin
D
Relative axin2 mRNA expression level
Relative lef1 mRNA expression level
Relative cyclinD1 mRNA expression level
*
WT Control
rapgef1b KD
E
% Phenotype
P2
P1
P0
WT control
DMSO control
rapgef1b ATG-MO (MO)
MO + mRNA
MO + Wnt inhibitor
mRNA + Wnt inhibitor
Wnt Inhibitor
Wnt Activator
MO + Wnt activator

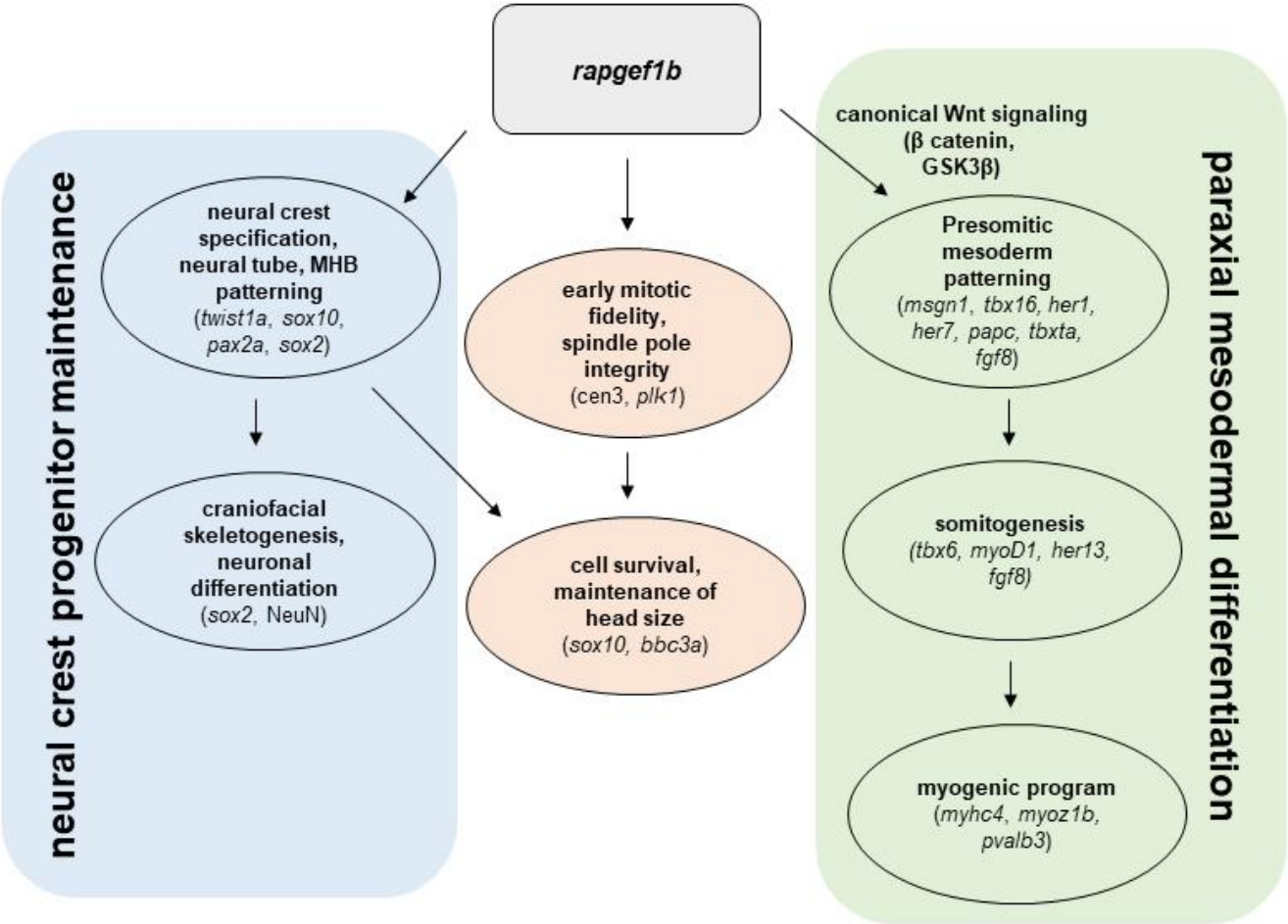
rapgef1b
neural crest progenitor maintenance
neural crest specification, neural tube, MHB patterning (twist1a, sox10, pax2a, sox2)
craniofacial skeletogenesis, neuronal differentiation (sox2, NeuN)
early mitotic fidelity, spindle pole integrity (cen3, plk1)
cell survival, maintenance of head size (sox10, bbc3a)
canonical Wnt signaling (β catenin, GSK3β)
paraxial mesodermal differentiation
Presomitic mesoderm patterning (msgn1, tbx16, her1, her7, papc, tbxta, fgf8)
somitogenesis (tbx6, myoD1, her13, fgf8)
myogenic program (myhc4, myoz1b, pvalb3)

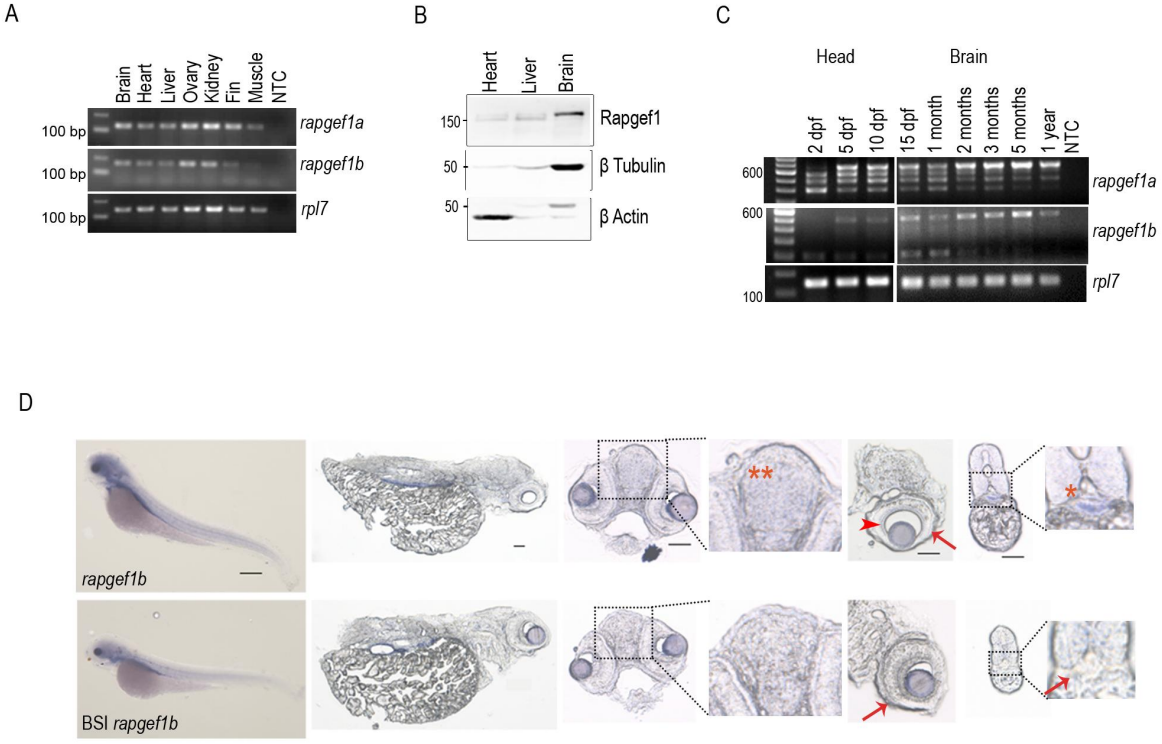
A
Brain
Heart
Liver
Ovary
Kidney
Fin
Muscle
NTC
100 bp
rapgef1a
100 bp
rapgef1b
100 bp
rpl7
B
Heart
Liver
Brain
150
Rapgef1
50
β Tubulin
50
β Actin
C
Head
Brain
2 dpf
5 dpf
10 dpf
15 dpf
1 month
2 months
3 months
5 months
1 year
NTC
600
rapgef1a
600
rapgef1b
100
rpl7
D
rapgef1b
BSI rapgef1b
**
*

A

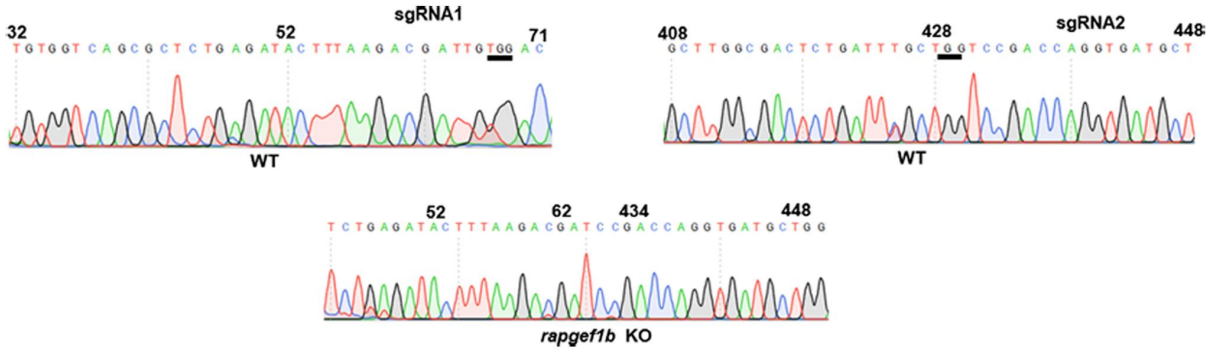
sgRNA1
32
52
71
WT
sgRNA2
408
428
448
WT
52
62
434
448
rapgef1b KO

B

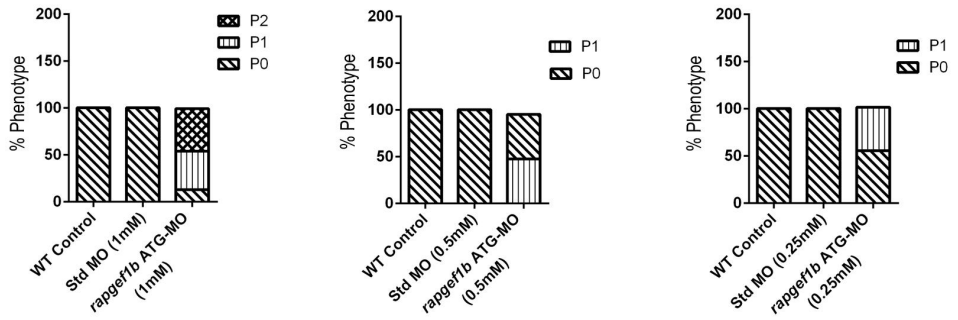
% Phenotype
P2
P1
P0
WT Control
Std MO (1mM)
rapgef1b ATG-MO (1mM)
Std MO (0.5mM)
rapgef1b ATG-MO (0.5mM)
Std MO (0.25mM)
rapgef1b ATG-MO (0.25mM)

C

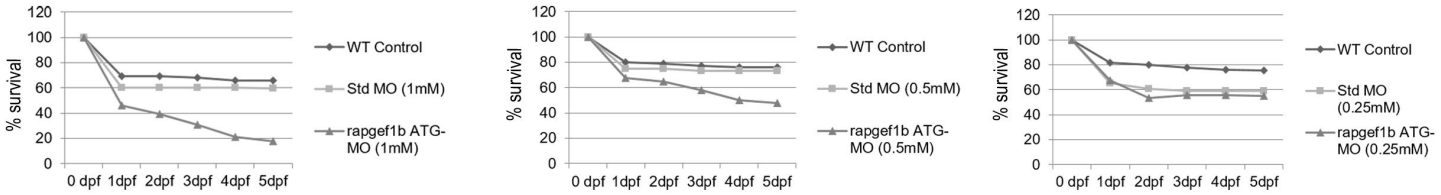
% survival
0 dpf
1dpf
2dpf
3dpf
4dpf
5dpf
WT Control
Std MO (1mM)
rapgef1b ATG-MO (1mM)
Std MO (0.5mM)
rapgef1b ATG-MO (0.5mM)
Std MO (0.25mM)
rapgef1b ATG-MO (0.25mM)

D

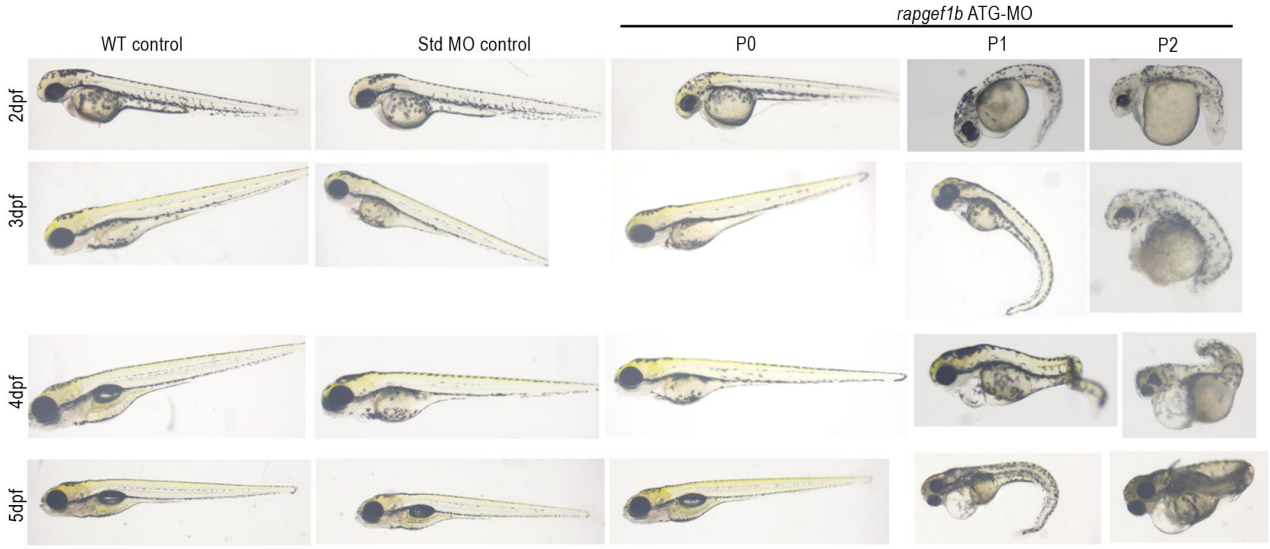
rapgef1b ATG-MO
WT control
Std MO control
P0
P1
P2
2dpf
3dpf
4dpf
5dpf

A

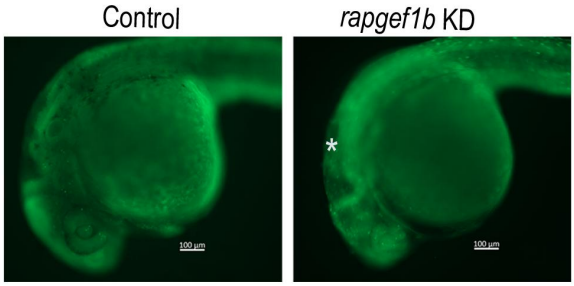
Control
rapgef1b KD
*
100 µm
100 µm

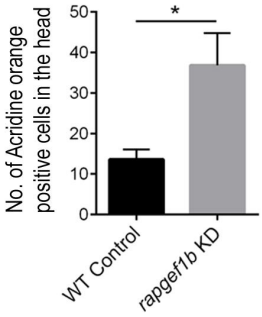
No. of Acridine orange positive cells in the head
50
40
30
20
10
0
*
WT Control
rapgef1b KD

B

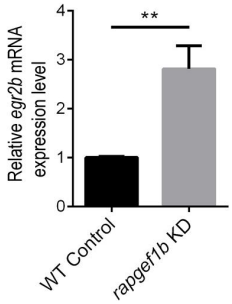
Relative egr2b mRNA expression level
4
3
2
1
0
**
WT Control
rapgef1b KD

C

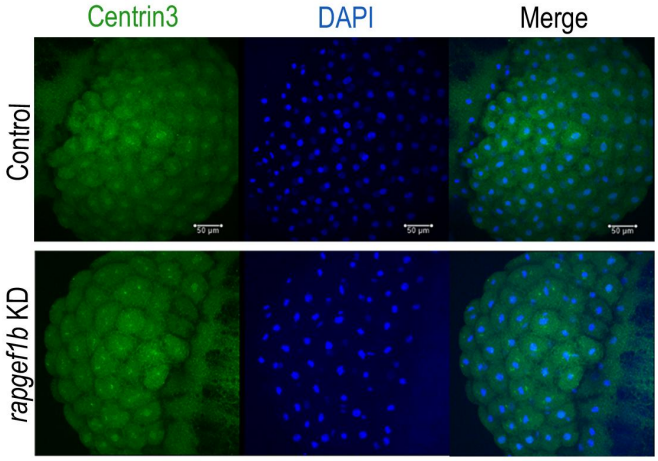
Centrin3
DAPI
Merge
Control
rapgef1b KD
50 µm
50 µm
50 µm

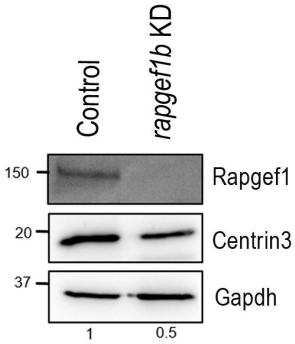
Control
rapgef1b KD
150
20
37
Rapgef1
Centrin3
Gapdh
1
0.5

D

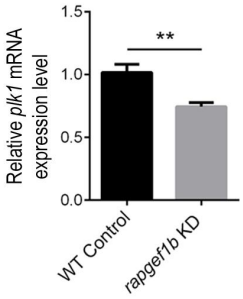
Relative plk1 mRNA expression level
1.5
1.0
0.5
0.0
**
WT Control
rapgef1b KD

Prasad_S4

A

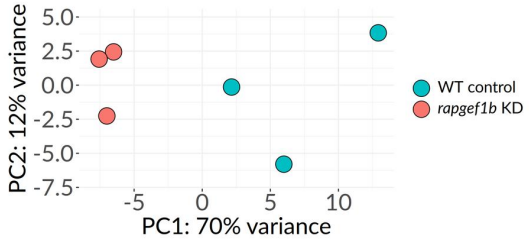

B

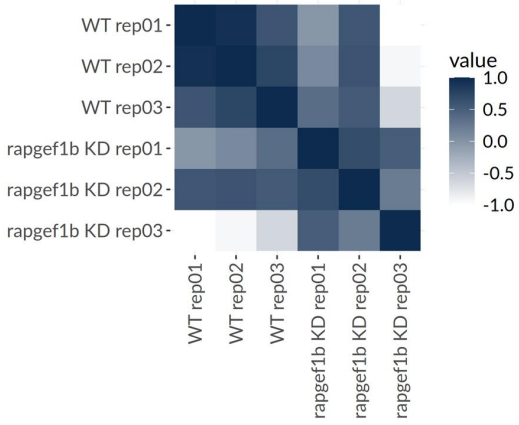

C

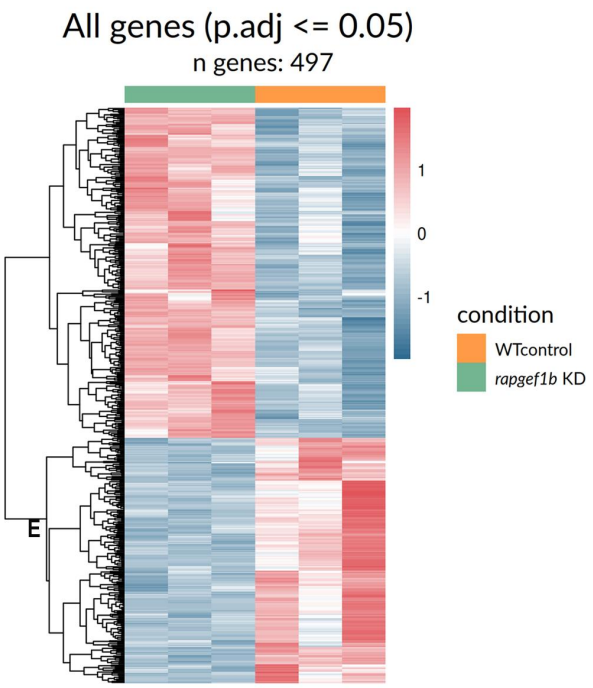

D

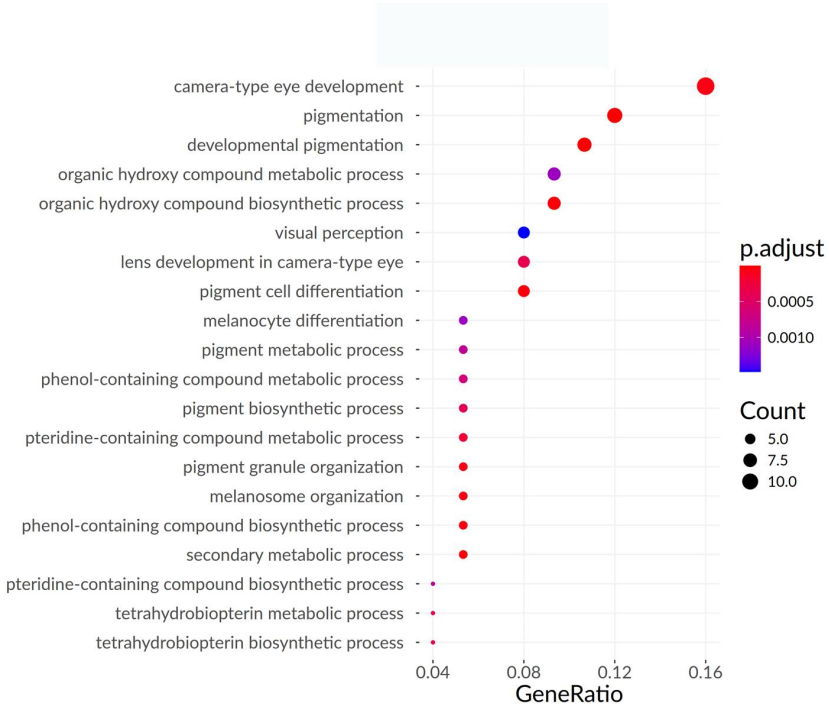

Table S1: List of all the primers used in the study.

Primer name	Forward primer (5′→ 3′)	Reverse primer (5′→ 3′)	Purpose
*rapgef1a*_Nter	CAAGATGGCGGTGGACAAGAA	GAGACAGGAGGACACCCTTGA	PCR
*rapgef1b*_Nter	GGACCCGCTGCATCAAAATG	TGAGACTTCTGGGATTCGTGC	PCR
*rapgef1b*_NISH	GACCCCATCTAAGAAAGG	CGTCGAGGTCGATGCCCT	ISH
*rapgef1a*_ISO	CGCCATATCCTGAAATACATGC	ATCAGGGCCGTCGTCGT TCT	PCR
*rapgef1b*_ISO	TCAACGACTCCTACAGCAGC	TGATAAAGATTCAGTGCGGTG	PCR
*rapgef1b*_KO	GGAGAAGGATGTGGTCAGCG	GGGGACGGTTGGTCATGTTT	KO PCR
rpl7	CTGTAGGGATAATGGCGGGTG	GTGACTTTGCTGGCCTTCTTG	PCR
beta Actin	CTCTTCCAGCCTTCCTTCCT	CACCGATCCAGACGGAGTAT	PCR
twist1a	GCCCGGTACATTGACTTCCT	TCAGGCCGAGAATCATGC	ISH
sox10	CACCACCCTCACGCTACAG	TCCACGTTACCGAAGTCGATG	ISH
pax2a	GCTGGAATGGTCCCTGGAAG	AACTTAATAACGCGGGGTTGCT	ISH
sox2	CGAGTCTAGTTCGAGTCCGC	GTTAATCGTCGTACCGGGCA	ISH
tbxta	AGACGAATGTTTCCCGTGCT	TCTGTCCTCCTCCGTTGAGT	ISH
myoD1	GCTGCCCAAAGTGGAGATTC	ATTATTCCGTGCGTCAGCATT	ISH
tbx6	CAACGCACTGATGGATGAAACC	GCGTTGAGGACACCACAGAA	qPCR
cdx4	AGTCGTCATCAACCGGCAAAA	TTCCTTAGCTCTGCGGTTCTG	qPCR
cdx4	TGGAGAAAGAGGCAAGCATGT	CTTCGTTCTCGTTTTGCCGGT	ISH
tbx6	AGTCATGTGACCCATGTGATTCC	ACAAGCAGGGATTGATTGGAAAGGT	ISH
axin2	GCTACAGGTCCTACAGACGCA	GAGTCATCCGTCAGGGCATC	qPCR

lef1	CCGCACAAGGAGCAAATCTTC	ACTGTCTAGCTGCGTCGTGA	qPCR
cyclinD1	AACTTCATCGCAAGCCCTCC	GATCGCAGACAGTCAGGGTCA	qPCR
her1	CTGCGAGAGATCAAGGCGATT	GCAGGGCACAGAGAGATACG	ISH
her7	AATCAAAATGGACAGAAAGCTGTTA	TCTGCTCGCTTGTGGTTCTT	ISH
papc	TCAGCTGAAATCCCAATTCCG	GATCAGTGGTGCCGCTTCTTT	ISH
fgf8	TTGCTACTATGCTCAGGTAACCA	GAGTAGCGGGTGCGTTTAGT	ISH
pvalb1	CTCCTTTGCTTTTCACTCGCC	TGTAGTCGAAGGAGTCGGCA	qPCR
myhc4	ACAAGCCAACTCTCACCTGTC	CCCTTCACTCTTCTTTGGCCTTTC	qPCR
myoz1b	GTGACGAGAACCTGTTGAACCT	AGCTCGTTCCCAAGGCGATA	qPCR
her13	GGATCTCAGGACATTGCTCACA	GAGTCACAGTCCCAGTTTCCTG	qPCR
tbx16	GAACAAACTCTAAAAGGCGGGC	CACCTCCAGCTCTTTACGGC	qPCR
msgn1	TGGAGGAACGTTTGCTCATCAT	AGACACCGACACTCCACTCA	qPCR
egr2b	GCGAGTGCTTCTTAGGACTTCA	TTAATCAGGCCATCTCCTGCG	qPCR
bbc3	CCGAACCATTGCCACTCAAA	CACTTCCTGTTCTGTTCCTGA	qPCR

Table S2: List of all the antibodies used in the study.

Antibodies	Dilutions	Catalog number	Purpose
C3G 3F6mAb		in-house generated (3F6) using the CBR domain of C3G	WB
mouse anti-β tubulin	1:2000	MA5-16308	WB
mouse anti-β actin	1:1000	MA5-15739	WB
mouse anti-GAPDH	1:2000	MA5-15738	WB
anti-Mouse IgG peroxidase conjugate	1:10 000	A4416	WB
mouse anti-α tubulin	1:100	DM1A mAb # 3873	IHC
rabbit anti-γ tubulin	1:2000	PA5-34815	IHC
rabbit anti-centrin3	1:100	PA5-96938	WB+IHC
mouse anti-β catenin	1:200	13-8400	WB+IHC
neuN	1:200	ab104224	IHC
donkey anti-rabbit Alexa Fluor 488	1:500	A-21206	IHC
donkey anti-mouse Alexa Fluor 568	1:500	A 10037	IHC
sheep anti-digoxygenin-AP, Fab fragments	1:5000	11093274910	ISH
rabbit anti- GSK3β	1:1000	CST#12456	WB
rabbit anti-pGSK3β (ser9)	1:1000	CST#5558	WB
rabbit p-β-Catenin (Ser33/37)	1:1000	CST#2009	WB